國立交通大學

材料科學與工程研究所

碩士論文

合成不同型態的氧化亞銅粒子探討其用於電化學還原二氧化碳及光催化甲基橙之能力

Synthesis of Cu_2O Particles in Various Morphologies for Electrochemical Reduction of CO_2 and Photocatalytic Decomposition of Methyl Orange

研究生：張庭瑜

指導教授：吳樸偉 博士

中華民國九十七年六月

合成不同型態的氧化亞銅粒子探討其用於電化學還原二氧化碳及光催化甲基橙之能力

Synthesis of Cu_2O Particles in Various Morphologies for Electrochemical Reduction of CO_2 and Photocatalytic Decomposition of Methyl Orange

學生：張庭瑜 Student: Ting-Yu Chang

指導教授：吳樸偉博士 Advisor: Dr. Pu-Wei Wu

國立交通大學

材料科學與工程研究所

碩士論文

A Thesis
Submitted to Department of Materials Science and Engineering
College of Engineering
National Chiao Tung University
in partial Fulfillment of the Requirements
for the Degree of
Master
in
Materials Science & Engineering
June 2008
Hsinchu, Taiwan, Republic of China

中華民國九十七年六月

合成不同型態的氧化亞銅粒子探討其用於電化學還原二氧化碳及光催化甲基橙之能力

學生: 張庭瑜　　指導教授: 吳樸偉 博士

國立交通大學 材料科學與工程研究所

中文摘要

利用化學還原法可以生成顆粒大小均一度的氧化亞銅粒子。我們使用分子量為 200 的聚乙烯做為界面活性劑、抗壞血酸鈉做為還原劑，並藉由氫氧化鈉調整反應溶液的酸鹼度以獲得不同粒徑的氧化亞銅粒子。

將氧化亞銅粒子塗布在商用氣體擴散電極上，在電解液中輸入二氧化碳，由此觀察氧化亞銅的催化活性。為了瞭解催化劑的顆粒大小以及電解液對於電化學還原二氧化碳的影響，取用直徑分別為 170、640 及 1570 nm 的氧化亞銅粒子，選擇碳酸氫鈉、氫氧化鈉及氯化鈣做為電解液。我們得知氧化亞銅對於電化學還原二氧化碳具有一定的催化能力。持續通入二氧化碳以及-1.7 V 的電壓 5 小時，640 nm 的氧化亞銅粒子在 0.5 M 氫氧化鈉水溶液中可以獲得最高的電流 (-4.82 $mAcm^{-2}$)。

探討氧化亞銅粒子做為光催化劑的光催化反應中，粒子形態及光源對光催化反應的影響，分別取用直徑為 170、640 及 1570 nm 的氧化亞銅粒子做為光催化劑，並改變光源，分別使用一盞 150 W 鹵素燈、四盞 27 W 白光日光及兩盞 27 W 白光日光燈。170 nm 的氧化亞銅例子顯現最佳的光催化能力，在 150 W 鹵素燈照射下 6 小時，有 31.7 % 甲基橙降解。

Synthesis of Cu_2O Particles in Various Morphologies for Electrochemical Reduction of CO_2 and Photocatalytic Decomposition of Methyl Orange

Student: Ting Yu Chang Advisor: Dr. Pu Wei Wu

Department of Materials Science and Engineering

National Chiao Tung University, Hsinchu, Taiwan, ROC

Abstract

Uniform Cu_2O particles with various sizes and shapes were prepared by chemical reduction route, in which the polyethylene glycol (PEG) with average molecular weight of 200 was adopted as the surfactant, the L-ascrobic acid sodium (LAAS) was employed as the reducing agent, and the NaOH was used to adjust the pH value of the solution.

We studied the electrochemical reductions of CO_2 on Cu_2O catalyzed gas diffusion electrodes to determine the catalytic abilities of the Cu_2O. Three different sizes of the monodispersed Cu_2O particles with diameters of 1570, 640, and 170 nm were explored as the catalysts. The $NaHCO_3$, NaOH, and $CaCl_2$ were chosen as the electrolytes. The Cu_2O particles presented moderate catalytic abilities for electrochemical reduction of CO_2. The highest average current density recorded was -4.82 $mAcm^{-2}$ with Cu_2O particles of average diameter of 640 nm in the 0.5 M NaOH electrolyte for 5 hours

electrochemical reduction of CO_2 at -1.7 V.

The effect for the morphologies and light sources on the photocatalytic abilities of Cu_2O was discussed. The Cu_2O particles with diameters of 1570, 640, and 170 nm were chosen as photocatalysts. Photocatalytic degradation of methyl orange in an aqueous solution containing those Cu_2O particles was investigated under one 150 W halogen lamp (yellow light), or two to four 27 W fluorescent lamp (white light). The photochemical process catalyzed by the Cu_2O particles with a diameter of 170 nm under single 150 W halogen lamp demonstrated the highest photocatalytic ability, in which 31.7 % methyl orange was decolorized after 6 hours irradiation.

Acknowledgement

哇！不知不覺兩年的研究所生活，就要告一段落啦！兩年的求學生活裡，要感謝的人，好多好多。首先，一定要感謝我的指導教授，吳樸偉老師，除了給我課業、實驗上的指導，也常常關心學生平時的生活、未來的生涯規劃。接著，感謝實驗室的學長姐們，勝結大哥、Kiokio 學長、張雲閔學長、黃苡叡學長、Kiki 學長、林老師實驗室的映眉學姊、小蔡學長及朝老師實驗室的欣君學姊，在課業、實驗上的指導以及平時的照顧。感謝我的好同學們，好滿足三人組之小錚及小均、朝老師實驗室的小媛及林老師實驗室的小柚，與我討論實驗、分享食物、天南地北地聊天。另外，感謝阿夢學妹、境妤學妹、馬特先生、澳洲魚丸小姐、三角學妹以及和成學弟，謝謝你們的幫忙唷！實驗室美好的未來就靠你們啦！還要感謝口試委員黃暄益老師以及林鵬老師，給予我論文及實驗上的指導與建議。

最後，要感謝親愛的爹地、媽咪，每天用 Skype 陪我分享生活的點點滴滴，在我沮喪的時候，給我滿滿的鼓勵，感謝親愛的珠妃麗小姐，為我的生活帶來許多歡笑，感謝蕭忠仁先生，除了協助我解決實驗上的問題，也與珠妃麗小姐一樣，讓我的生活充滿歡樂。

謝謝大家，因為有你們，我才能擁有快樂充實的研究所生活。

Table of Contents

List of Figures

List of Tables

Chapter1.

Introduction

1.1. Motivation

Our life has become more convenient and comfortable ever since the industrial revolution. Unfortunately, there is a price that accompanies the rising living standard, which is the worsening greenhouse effect. The greenhouse effect is a process that makes the surface temperature of earth warmer every year. Among many possible suspects, the carbon dioxide is the primary cause. Hence, there is an urgent need to identify an effective method to reduce the concentration of carbon dioxide in the atmosphere in order to mitigate the greenhouse effect.

To date, there are extensive researches in identifying the appropriate method to reduce the carbon dioxide concentration in the atmosphere. For example, approaches such as chemical absorption, physical adsorption, bioconversion, and electrochemical conversion have been investigated. Since our laboratory is known for electrochemical applications, it becomes our objective to study practical means of CO_2 reduction in electrochemical route.

In this study, we synthesized cuprous oxide nanoparticles in different sizes and shapes by a variety of chemical synthetic methods. The as-synthesized powders were used as the electrocatalyst dispersed on a gas diffusion electrode to activate CO2 reduction when immersed in a proper electrolyte. In addition, we studied the effects of shape and size of the cuprous oxide on the resulting CO_2 catalytic behaviors. Furthermore, we explored possible photocatalytic

abilities for the Cu_2O. This thesis documents our preliminary efforts in Cu_2O material synthesis and application evaluations.

1.2. Background of cuprous oxide

1.2.1. Materials characteristics of cuprous oxide

The Cu_2O began to attract considerable interests in 1920s since invention of the cuprous oxide rectifier was demonstrated by Grondhal et al.[1] Afterwards, many characterizations of Cu_2O were carried out and reported from 1930 to 1940.[1] Typically, the Cu_2O is found in red colored rocks. However, it is likely to reveal many other colors from red to yellow and the color of Cu_2O is influenced greatly by its particle sizes.

The Cu_2O is insoluble in organic solvents and water but it can be dissolved in hydrochloric acid to form $HCuCl_2$. In addition, in electrolytes of dilute nitric acid and sulfuric acid copper(II) sulfate and copper(II) nitrate are formed, respectively. Moreover the Cu_2O could be dissolved in concentrated ammonia solution to form $[Cu(NH_3)_2]^+$ and the latter oxidizes to $[Cu(NH_3)_4(H_2O)_2]^{2+}$ readily. The melting point of Cu_2O is about 1235 °C and its density is about 6.0 gcm^{-3}.[2]

The Cu_2O is known as a semiconductor with a direct band gap about 2.14 eV. Intrinsically, it is a P-type semiconductor which is due to the presence of copper vacancies. The resistivity for Cu_2O is found to vary from a few tens of Ω. cm to 10^4 Ω. cm. The crystal structure of Cu_2O is cuprite with a lattice constant of 4.27 Å. The oxygen anions are arranged in a body-centered relatively to each other and the copper cations are positioned in a face-centered

lattice. [1]

1.2.2. Synthesis of cuprous oxide

A. Electrodeposition

Stareck et al. conducted the earliest research in which electrodeposition was employed to fabricate an uniform film of Cu_2O. Generally speaking, the Cu_2O could be electrochemically deposited onto conductive substrates such as gold and indium-doped tin oxide. The applied potential between the anode and cathode is typically less than 0.5 V and the growth conditions determine the morphologies of the resulting films. [1]

Previously, Yan et al. selected anionic surfactant sodium bis(2-ethylhexyl) sulfosuccinate (AOT), oil phase *p*-xylene, and $CuCl_2$ to form cuprite nanowires. The electrodeposition was performed at a static potential of -1.1 V for 1 or 2 hours with two copper electrodes as working and counter electrodes, respectively. A large number of nanowires with 3 to 5 μm in lengths and 25 to 45 nm in diameters were obtained at a deposition time of 1 hour. They reported that increasing the deposition time to 2 hours resulting in nanowires longer than 10 μm with average diameters of 100 nm.[3]

Recently, Wang et al. deposited the Cu_2O on indium-doped tin oxide (ITO) substrate via an electrodeposition with a potential of -0.2 V against the Ag/AgCl for 600 seconds. The electrolyte was a mixture of cetyl trimethylammonium bromide (CTAB), NaAc, and $Cu(Ac)_2$. They

obtained flower-leaves to cactus Cu_2O through controlling the concentrations of CTAB. They observed that by increasing the concentration of CTAB the flower-leaves Cu_2O became cactus shaped (shown in figure 1.2).[4]

B. Chemical reduction

Chemical reduction is a relatively simple method to form Cu_2O with unique shapes and sizes. It has been established that the identification of suitable surfactants, reducing agents, copper(II) ion sources, and processing parameters is critical in synthesizing Cu_2O with superb uniformity.

Wang et al. synthesized Cu_2O nanowires at room temperature using the $CuCl_2$ as a copper(II) ion source, hydrazine as a reducing agent, and PEG (M.W. 20000) as a surfactant. The NaOH solution was added into the solution containing $CuCl_2$ and PEG to form $Cu(OH)_2$ as blue precipitates. After adding the hydrazine into the solution containing $Cu(OH)_2$, they obtained Cu_2O nanowires. The diameters of the nanowires were about 8 nm and the length of the nanowires ranges from 10 to 20 μm.[5]

Murphy et al. not only changed the adding sequence of base (NaOH) and reducing agent (L-ascorbic acid, AA), but also controlled the concentration of surfactant (PEG with M.W. 600) to prepare the Cu_2O nanocubes with various edge lengths from 25 to 200 nm. They observed that when the reducing agent (AA) was added into $CuSO_4$ solution before hydroxide, varying the concentration of PEG was not

affect the particle size of the Cu_2O nanocubes. However, when the AA and base were added simultaneously, decreasing the concentration of PEG from 0.025 to 0.0031 M led to smaller particle sizes with uniform cubic morphologies (shown in figure 1.3).[6]

Chen et al. used the PEG as a reducing agent and gelatin as a soft template to synthesize spherical Cu_2O with nanoholes. They prepared the Cu_2O by heating the mixture of $CuSO_4$, PEG, and gelation at 70 °C and then adding the NaOH solution into the mixture drop by drop. The hollow Cu_2O spheres with diameters about 100 to 200 nm were obtained with a titration rate of 4 $mLmin^{-1}$ for the NaOH solution. When they adjusted the titration rate to 0.25 $mLmin^{-1}$, the hollow Cu_2O spheres became much larger (with diameter about 600 nm, shown in figure 1.4).[7]

Recently, Huang et al. used the sodium dodecyl sulfate (SDS) as a capping agent and sodium ascorbate (SA) as a reducing agent to fabricate the Cu_2O nanoparticles by the seed-mediate method. The $CuSO_4$ and SDS were first mixed thoroughly and the SA and NaOH were added subsequently. The as-prepared seed nanoparticles were transferred into another vessel containing $CuSO_4$ and SDS followed by addition of SA and NaOH. Through the unique seed-mediated route they prepared monodispersed Cu_2O particles with adjustable sizes ranging from 40 to 420 nm (shown in figure 1.5). [8]

C. Hydrothermal reduction

Hydrothermal synthesis is a particular method of growing single

crystals at relatively high pressure. Zhu et al. prepared hollow Cu_2O microspheres about 10 μm in diameter with nanocrystals-composed porous multishells by solvothermal synthesis. They added copper nitrate and glutamic acid into ethanol simultaneously and transferred the mixture to a Telfon-lined stainless autoclave followed by heat treatment at 160 °C for different duration. They obtained copper hydroxynitrate hollow microspheres with well crystallinity, after 2 hours of solvothermal treatment. When the solvothermal time was prolonged to 48 hours, the copper hydroxynitrate hollow microspheres were totally transformed to Cu_2O microspheres with impressive multilayer hierarchy (shown in figure 1.6). [9]

Sun et al. developed a similar hydrothermal process to synthesize Cu_2O by reducing copper-citrate complex directly. The procedure for Cu_2O preparation was mixing $Na_3C_6H_5O_7$, $CuCl_2$, and NaH_2PO_2 simutaneously, followed by heating in the Teflon-lined autoclave at 100 °C for 24 hours. By adjusting the pH value of the solution with NaOH they were able to obtain a variety of Cu_2O particles. They obtained Cu_2O cubes with particle size about 1 μm at a pH value of 6.5. When they increased the pH value to 8.0, they observed eight-pod particles with particle size about 2 μm (shown in figure1.7).[10]

Wei et al. also synthesized pure copper nanocrystallites with sizes ranging from 50 to 100 nm and Cu_2O nanorods via a solvothermal treatment. The typical size of Cu_2O nanorods is 10 to 15 nm in width and 20 to 50 nm in length. Pure copper nanocrystallites were prepared by $CuSO_4$ or $CuSO_4 \cdot 5H_2O$, with NaOH in ethanol at 140 °C for 10 hours. In contrast, the cuprous oxide nanorods were prepared by $CuSO_4$ or

$CuSO_4$. $5H_2O$, with NaOH in a mixed solution containing ethanol and deionized water at 140 °C for 10 hours (shown in figure 1.8). [11]

In addition to the above-mentioned report, Valtiera et al. adopted the 2,4-pentanedionate copper(II) as a precursor and chose the vapor deposition method to grow Cu_2O film on fiberglass.[12] The Cu_2O film was formed by thermal oxidation under suitable conditions.[1]

1.2.3. Applications of cuprous oxide

There have been strong interests in the Cu_2O because it is a material with merits such as low cost, simple preparations into various shapes, and promising applications.

First, the Cu_2O acts as a reasonable photo catalyst for water splitting into oxygen and hydrogen under visible light irradiations. Domen et al. prepared the Cu_2O by the hydrolysis of CuCl. Afterwards, they illuminated the as-prepared Cu_2O in distilled water by a 300 W Xe lamp for more than 1900 hours. To their surprise, they observed that the photocatalytic water splitting on the Cu_2O powders demonstrate negligible reduction in the activity for more than 1900 hours.[13]

Second, the Cu_2O exhibits high sensitivities to some flammable gases. Li et al. prepared the Cu_2O nanoparticles in 200 nm by chemical reduction of copper. Some of the as-prepared nanoparticles were subjected to an annealing at 500 °C for 1 to 2 hours to form CuO nanospheres and the others were under aging at room temperature for 0.5 to 3 min forming nanospheres. They determined that the Cu_2O nanospheres reveal higher sensitivities than that of the CuO nanospheres. [14]

Third, the Cu_2O can be used in photo degradation of selective dye molecules. Wang et al. reduced the $CuCl_2$ by hydrazine and obtained different shapes and sizes of Cu_2O through adjusting the concentrations of NaOH and NH_3. They reported that the octahedral Cu_2O adsorbs 80 % methyl orange under a 500 W Hg lamp for 30 minutes. On the other hand, the cubic Cu_2O demonstrates much less degradation ability for the methyl orange.[15]

Lastly, the Cu_2O is believed to exhibit moderate ability in solar energy conversion.[1] Minami et al. combined an n-type ZnO thin film with a p-type Cu_2O thick sheet by methods such as magnetron sputtering (MSP), pulsed laser deposition (PLD), and vacuum arc plasma evaporation (VAPE). They reported that a Ga-doped ZnO-Cu_2O heterojunction solar cell fabricated by a ZnO thin film prepared by VAPE and an Al-doped ZnO-Cu_2O device fabricated using PLD exhibit efficiencies of 1.52 and 1.42 % using AM2 solar illumination (100 $mWcm^{-2}$).[16]

In addition, considerable interests have arisen on the Cu_2O for novel applications, including the anode material for lithium ion battery[17] and catalyst for CO conversion.[18]

1.3. Methods in carbon dioxide reduction

In order to avoid the disaster brought by greenhouse effect, numerous methods have been suggested to reduce the CO_2 concentration in the atmosphere. In following section, we would discuss two of the most popular methods of CO_2 sequestration.

1.3.1. Absorption/Adsorption

There are many absorbents available to retain CO_2. They include polymer membranes, zeolites, perovskites, magnesia, and sodalime. Pfeiffer et al. used commercial Li_2O to absorb CO_2 at different temperatures. Result from the thermogravimetric analyses (TGA) on the Li_2O in a CO_2 flux indicated an increase of weight about 14.3 wt% between 190 and 400 °C due to Li_2O conversion into Li_2CO_3. When the reaction temperature was increased to 600 °C, more Li_2O became $LiCO_3$ and the weight increased dramatically raised to 226 wt% (86 mol%), corresponding to 1.26 g of CO_2 per gram of Li_2O. Figure 1.9 depicted the mechanism proposed for the CO_2 absorption on Li_2O and the SEM image of Li_2O before and after heat treatment at 600 °C for 2 hours in a CO_2 flux. [19]

Pfeiffer et al. also prepared $Li_{2-x}Na_xZrO_3$ by a heat treatment of Li_2CO_3, Na_2CO_3, and $Zr(OCH_3)_4$ at 900 °C to absorb CO_2. They determined the CO_2 absorption of Na_2ZrO_3 was higher than that of Li_2ZrO_3. Results from the thermogravimetric analyses indicated that the Li_2ZrO_3 absorbed CO_2 with an increase of weight about 4 wt% after the reaction. Similarly, the $Li_{1.8}Na_{0.2}ZrO_3$ increased its weight to 6.9 wt% and $Li_{1.4}Na_{0.6}ZrO_3$ increased its weight to 13.1 wt%, respectively. Comparing to other samples they prepared, the $LiNaZrO_3$ demonstrated the highest CO_2 chemisorption efficiency of 75.3 % at 600 °C.[20]

Hausler et al. estimated the influence of SO_2, N-methyldiethanolamine (MDEA), and triethanolamine (TEA) on the CO_2 absorption capacity by utilizing aqueous 2-(2-aminoethylamino)ethanol (AEE) solution and its blends with MDEA and TEA to absorb CO_2 or CO_2/SO_2 mixtures at 23 °C. They

found out that the additions of 5 and 10 wt% of MDEA and TEA exerted negligible influence on the CO_2 absorption in AEE solution. Furthermore, adding MDEA increased the CO_2 absorption capacity of AEE slightly, whereas adding TEA decreased the CO_2 absorption capacity of AEE in the absence or presence of SO_2. They obtained the highest CO_2 absorption capacity about 1.267 mol of CO_2 per mol of amine by using 15 wt% AEE + 10 wt% MDEA.[21]

In order to determine the best adsorbent for CO_2, Snap et al. prepared nitrogen enriched carbons by urea-formaldehyde (UF) and melamine-formaldehyde (MF) in the presence of K_2CO_3. The K_2CO_3 acted as a chemical activation agent activating the reaction over a range of temperatures from 400 to 700 °C. The UF with an activation temperature of 500 °C presented the highest CO_2 capacity, capturing over 8 gram CO_2 per 100 gram of adsorbent at 25 °C. Higher activation temperature resulted in higher surface area, but did not improve CO_2 capturing ability, suggesting that sites suitable for the adsorption of CO_2 were destroyed at higher temperature.[22]

1.3.2. Electrochemical reduction

Electrochemical reduction of CO_2 has attracted much attention because it might be a promising method for turning CO_2 to useful materials. Some common products of CO_2 from the electrochemical reduction are listed below. The equilibrium potentials of each reaction have been reported by Sullivan et al. under the standard conditions against NHE.[23]

$$2CO_2 + 2H^+ + 2e^- \rightarrow H_2C_2O_4 \qquad E^0 = -0.475 \qquad (1.1)$$

$$CO_2 + 2H^+ + 2e^- \rightarrow HCOOH \qquad E^0 = -0.199 \qquad (1.2)$$

$$CO_2 + 2H^+ + 2e^- \rightarrow CO + H_2O \qquad E^0 = -0.109 \qquad (1.3)$$

$$CO_2 + 4H^+ + 4e^- \rightarrow HCHO + H_2O \qquad E^0 = -0.071 \qquad (1.4)$$

$$CO_2 + 6H^+ + 6e^- \rightarrow CH_3OH + H_2O \qquad E^0 = +0.030 \qquad (1.5)$$

$$CO_2 + 8H^+ + 8e^- \rightarrow CH_4 + 2H_2O \qquad E^0 = +0.169 \qquad (1.6)$$

Fujishima et al. used various metal wires (Ti, W, Ni, Pd, Pt, Cu, Ag, Zn, Sn, and Pb) as the working electrode, Pt wire as the counter electrode, and 0.3 M tetrabutylamonium perchloride (TBAP) in methanol as a supporting electrolyte to conduct electrochemical reduction of CO_2 galvanostatically at 25 °C, 41 atm, mainly at 200 $mAcm^{-2}$. The electrochemical reduction products were analyzed by flame ionization detector (FID) and thermal conductivity detector (TCD). They found out that W, Ti, and Pt electrodes did not possess the required ability in electrochemical reduction of CO_2. Formate was produced at Sn and Pb electrodes, but much more CO was also observed. In contrast, electrolysis at Ag, Zn, and Pd electrodes yielded CO mostly. The Cu electrode revealed better ability to form hydrocarbons in aqueous electrolyte than in methanol system. However, the hydrocarbon formation at Ni electrode was more efficient in methanol than that of the aqueous system.[24]

Fujishima et al. also used RuO_2 deposited on boron-doped diamond (BDD) as the working electrode, the Pt used as the counter electrode, and SCE as the reference electrode to reduce CO_2. They adjusted the pH value of the solution by NaOH and they obtained the optimized efficiency for CO_2 reduction (almost 80 %) at pH of 4, which was close to saturated aqueous solution of carbonic

acid. The applied potential was -0.55 V and the current density was about -0.45 $mAcm^{-2}$. In their study, their found out the use of BDD as a substrate for the RuO_2 layers resulted in much lower Faradic efficiency for CO_2 reduction to methanol as compared to using the TiO_2 as a substrate.[25]

Hori et al. prepared the silver-coated ion exchange membrane (solid polymer electrolyte, SPE) electrodes through the electroless method to deposit silver onto the ion exchange membrane. The SPE electrode was used as the working electrode, a Pt plate was used as the counter electrode, and 0.2 M K_2SO_4 was adopted as the electrolyte. Ag/SPE prepared from an anion exchange membrane (AEM) reduced CO_2 to CO and HCOOH for more than 2 hours. They controlled the current density at 50 $mAcm^{-2}$ and obtained average electrode potential about -1.8 V (vs. SHE) when the reduction process was performed at the AEM electrode with silver coated two layers. However, the SPE electrode system prepared from the cation exchange membrane (CEM) was not suitable for CO_2 reduction, since OH^-, HCO_3^-, and CO_3^{2-} formed in the CO_2 reduction could not be removed from the metal membrane interface.[26]

Ogura et al. prepared copper(I) halide-confined Cu-mesh electrodes by electrochemical oxidation (applied potential: 0.2 to 0.4 V) of HCl, KBr, and KI, respectively. The electrolysis potential for the electrochemical reduction of CO_2 was -2.4 V (Ag/AgCl). When they used the CuCl as working electrode, they chose 3 M KCl as electrolyte and recorded current density about 46 $mAcm^{-2}$. When they used the CuBr as working electrode, they selected 3 M KBr as electrolyte and obtained current density about 37 $mAcm^{-2}$. Although the CuBr electrode presented lower current density, it conversed 24.3 % of CO_2 more than that of CuCl electrode (17.1 %). Table 1.1 presents the Faradaic efficiencies for the products obtained in the electrochemical reduction of CO_2

at -2.4 V (Ag/AgCl) on a copper(I) halide-confined Cu-mesh electrode. [27]

Köleli et al. used the electrodeposition method to deposit polypyrrole on the platinum as working electrode for electrochemical reduction of CO_2. The electrolyte was MeOH/0.1 M $LiClO_4/H^+/H_2O$, the applied potential was -0.4 V (Ag/AgCl) and the obtained current density was smaller than 13 $mAcm^{-2}$ under ambient condition. When the electrochemical process was operated under ambient condition, only a minute amount of CO_2 became HCOOH, CH_3COOH, and HCHO. However, they obtained much more HCOOH, CH_3COOH, and HCHO under high pressure (20 bar).[28]

Kaneco et al. used copper the electrode in methanol with sodium supporting salts to reduce CO_2 by electrochemical method. The reduction process was investigated with various sodium supporting salts, such as acetate, chloride, bromide, iodide, thiocyanate, and perchlorate, at a low temperature (-30 °C). The best results they obtained were utilizing 0.5 M $NaClO_4$ (methanol-based) electrolyte at -3.0 V (Ag/AgCl). The current density was 27 $mAcm^{-2}$ and the faradic efficiency of methane was 70.5 %.[29]

Koleli et al. studied the electrochemical reduction of CO_2 on Pb and Sn electrodes in aqueous $KHCO_3$ and K_2CO_3 electrolyte in a fixed-bed reactor. The highest current efficiency for formic acid, the predominant product, obtained in 0.5 M $KHCO_3$ at -1.5 V (SCE) after 30 min electrolysis was found to be 90 % for Pb electrode and 74 % for Sn electrode. Meanwhile, the current efficiency for the formic acid in 0.1 M K_2CO_3 at -1.5 V (SCE) after 30 min electrolysis was found to be 39 % for Pt electrode. Figure 1.10 depicted the image of the electrochemical fixed-bed reactor, the current-potential diagram and the Faradaic current efficiency–potential diagram for formic acid formation on Pb electrode in 0.1 M K_2CO_3 at different time intervals.[30]

1.4. Properties and applications of photocatalysts

Photochemistry is the subject studying the relationship between light and molecules. Light is the common name for electromagnetic (EM) radiation in the visible, near-ultraviolet, and near-infrared spectral range. The electromagnetic spectrum includes a variety of radiations from very long radio waves with the dimension of buildings to very short gamma rays which are much smaller than an atom nucleus. In the wave model, the frequency (λ) is inversely proportional to the wavelength (ν) according to the equation:

$$c = \lambda\nu \qquad (1\text{-}7)$$

The value of c is constant (2.998×10^{8} ms^{-1} in vacuum).[31]

In the quantum model, the photon is used to describe the quantized energy of an electromagnetic wave. A photon has no mass but it has a specific energy (E) directly proportional to the frequency (ν) of the radiation, according to the Planck relation:

$$E = h\nu \qquad (1\text{-}8)$$

Where h is the Pranck constant (6.626×10^{-34} J. s).[31]

The reactions induced by light are defined as photochemical reactions. The first step of a photochemical process is the photoexcitation (the mechanism of electron excitation by photon absorption), where the reactant is elevated to an excited state possessing a higher energy than that of ground state.

$$M + h\nu \rightarrow M^* \quad (1\text{-}9)$$

where M is the molecule at ground state, M* is the molecule at excited state, and hν is the photon energy. [31]

The molecule in the excited states could return to the ground state by various processes.

$$M^* \rightarrow M + h\nu' \quad (1\text{-}10)$$

$$M^* \rightarrow M + \text{heat} \quad (1\text{-}11)$$

$$M^* + Q \rightarrow M + Q' \quad (1\text{-}12)$$

where Q is the molecule that absorbed the excited energy of M*.

The photochemical reaction could be categorized by the usage of photosensitizing materials (photocatalyst). If the initial reactant could not absorb light energy or the light energy could not derive sufficient energy for photochemical reaction, the photocatalysts were added to absorb light and promote the desirable photochemical reaction. In principle, the photochemical reaction with photocatalysts added may proceed on the surface of a semiconductor through several steps. First, electron-hole pairs are created by exciting the semiconductor with light or suitable energy. Second, isolation of the electrons and holes on the semiconductor surface takes place. Third, the separated electrons and holes would initiate individual redox process with the reactants adsorbed on the surface. Finally, the products are released and the surface reconstructed.[31]

Yang et al. prepared the Cu_2O nanoparticles with diameter of 35 nm via the electrochemical method in alkaline NaCl solutions with copper as electrode

and $K_2Cr_2O_7$ as additive. Electrolysis was performed under stable current densities (50, 70, 90, 100, and 110 $mAcm^{-2}$) at 70 °C for 1 hour and the Cu_2O nanocrystal prepared under 100 $mAcm^{-2}$ was chosen as the catalyst. They observed thtat 97 % of 50 mgL^{-1} methyl orange (MO) was decomposed under a 125 W high-pressure mercury lamp for 2 hours or under sunlight for 3 hours when Cu_2O in $2gL^{-1}$ was added. In contrast, pure TiO_2 and CdS photocatalysts were effectively only under UV irradiation.[32]

Andronic et al. prepared the TiO_2 film by Spray Pyrolysis Deposition (SPD) in order to study the influence of the TiO_2 in specific surface (powder, film) on the photocatalytic degradation of MO. The photcatalysis process was operated under an 18 W fluorescence lamp by adding 1 g TiO_2 powder per 1 L solutions with different MO concentrations. At higher MO concentrations, the light penetration was reduced which was due to heavy MO adsorption on the TiO_2 and fewer photons were able to reach the catalyst surface. When the film and powder were 0.004 gL^{-1} and the MO was 7.8125 mgL^{-1}, the film of TiO_2 demonstrated photocatalytic efficiency about 5.10 % after 6 hours of reaction, this value was lower than that of TiO_2 (efficiency: 7.12 %).[33]

Liu et al. synthesized the $BiFeO_3$ (BFO) nanoparticles via a sol-gel method and studied their photocatalytic abilities through decomposition of MO. They dissolved bismuth nitrate and iron nitrate within 2-methoxyethanol and added polyethylene glycol as a dispersant. The mixture was calcinated under 500 °C for 2 hours to form perovskite-type BFO. The initial concentration for MO was 15 mgL^{-1} with a catalyst loading of 30 $mmolL^{-1}$ (11.545 gL^{-1}) and more than 90 % of MO was decolorized after 8 hours of irradiation under a 300 W Xe lamp. Figure 1.11 presents the photocatalytic ability of bulk and nanoparticlate BFO on degradation of MO under UV-vis light irradiation and

visible light irradiation. [34]

Parida et al. prepared the hydrated titanium oxide by a sol-gel approach, adopting titanium isopropoxide as starting material. The as-prepared TiO_2 nanoparticles were made into a series of sulfated TiO_2 samples via an aqueous wetness impregnation method with various weight percentages of SO_4^{2-}. The photocatalytic degradation of MO was carried out under sunlight with a solar intensity about 800 Wm^{-2} by taking 20 mL of 150 mgL^{-1} MO solution with 1.0 gL^{-1} catalyst. The samples loaded with 2.5 wt % SO_4^{2-} indicated higher degradation ability than without or less loading and its behavior may be due to the addition of sulfate that effectively decreased the crystal size of the TiO_2. By adjusting the pH value of the solution from 8 to 2, they found out the percentage of degradation was increased with decreasing pH values. Since the surface of the sulfate-modified TiO_2 became positively charged at pH lower than 4.5 to 5.0 and MO was an anionic dye, the photocatalytic reaction was likely to be faster at acidic pH. Figure 1.12 depicts the mechanisms occurring on the TiO_2 surfaces exposed to light for the photodegradation of organic pollutants.[35]

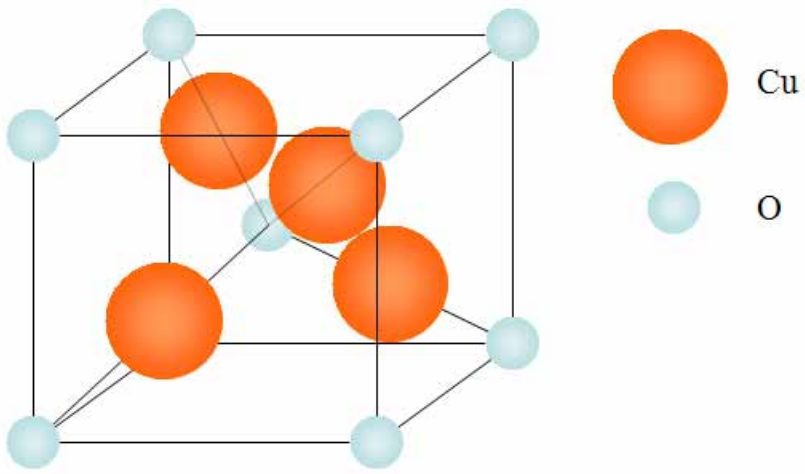

Figure 1.1. The crystal structure of Cu_2O.[1]

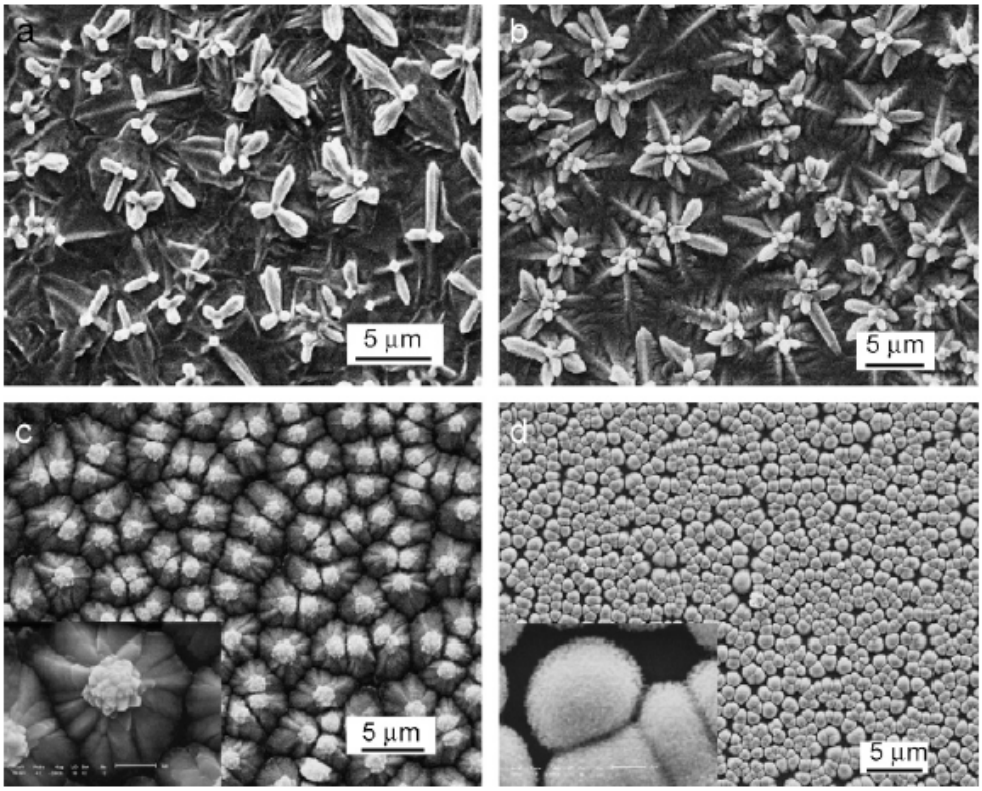

Figure 1.2. SEM images of Cu_2O deposited on ITO substrates from electrolyte containing 0.02 M $Cu(Ac)_2$, 0.1 M NaAc and CTAB with different concentrations: (a) 0, (b) 0.4 mM, (c) 0.8 mM, and (d) 2.8 mM.[4]

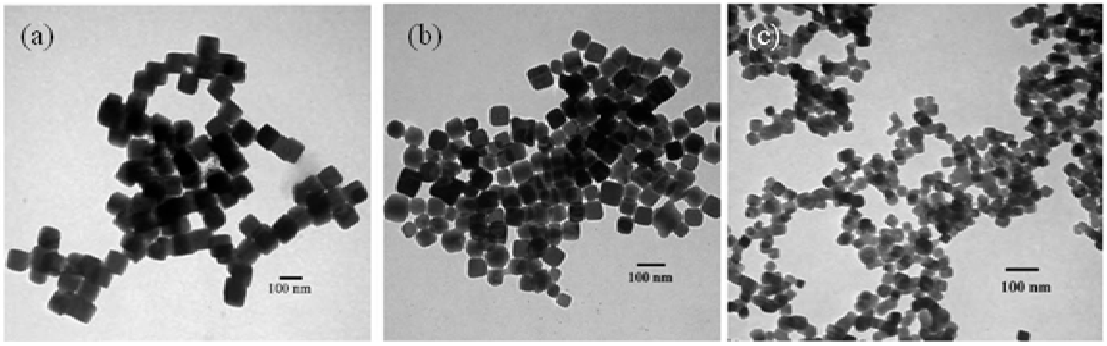

Figure 1.3. TEM images for Cu_2O nanocubes fabricated by adding the mixture of AA and NaOH into the solution containing Cu^{2+} and (a) 4 mL, (b) 2 mL, and (c) 1 mL of 0.05 M PEG.[6]

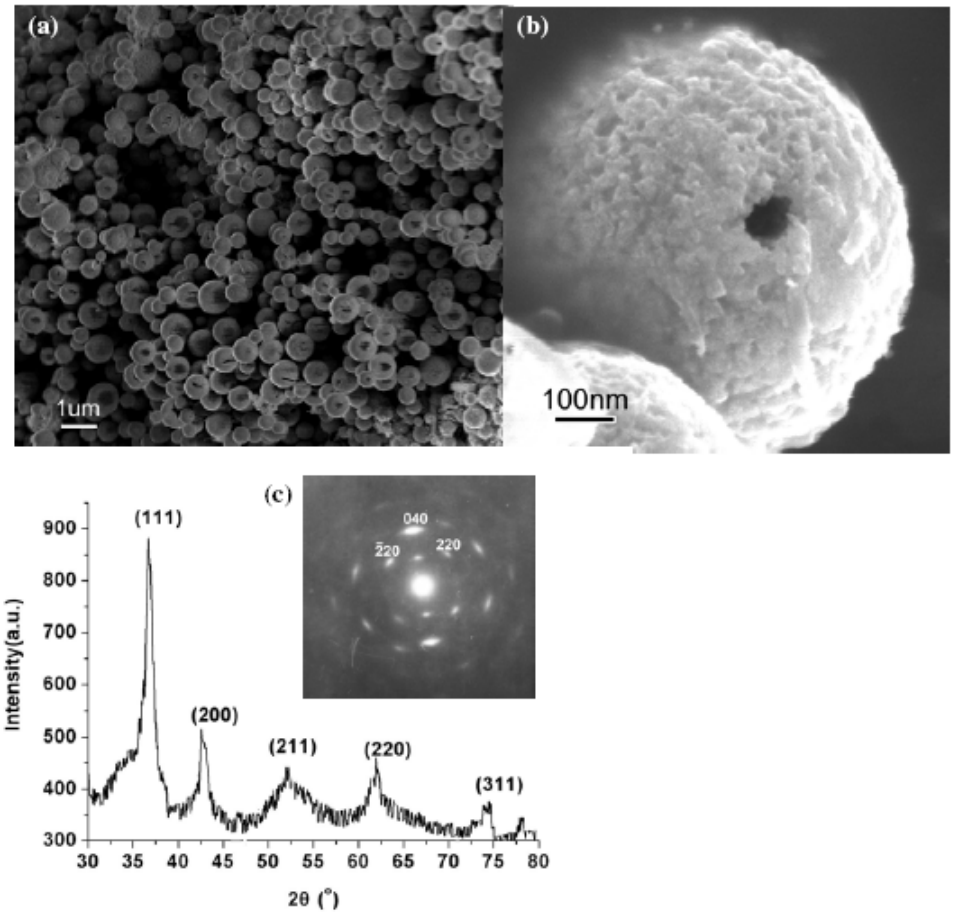

Figure 1.4. SEM images (a), (b), and XRD pattern (c) of hollow Cu_2O spheres produced with a NaOH titration rate of 0.25 $mLmin^{-1}$.[7]

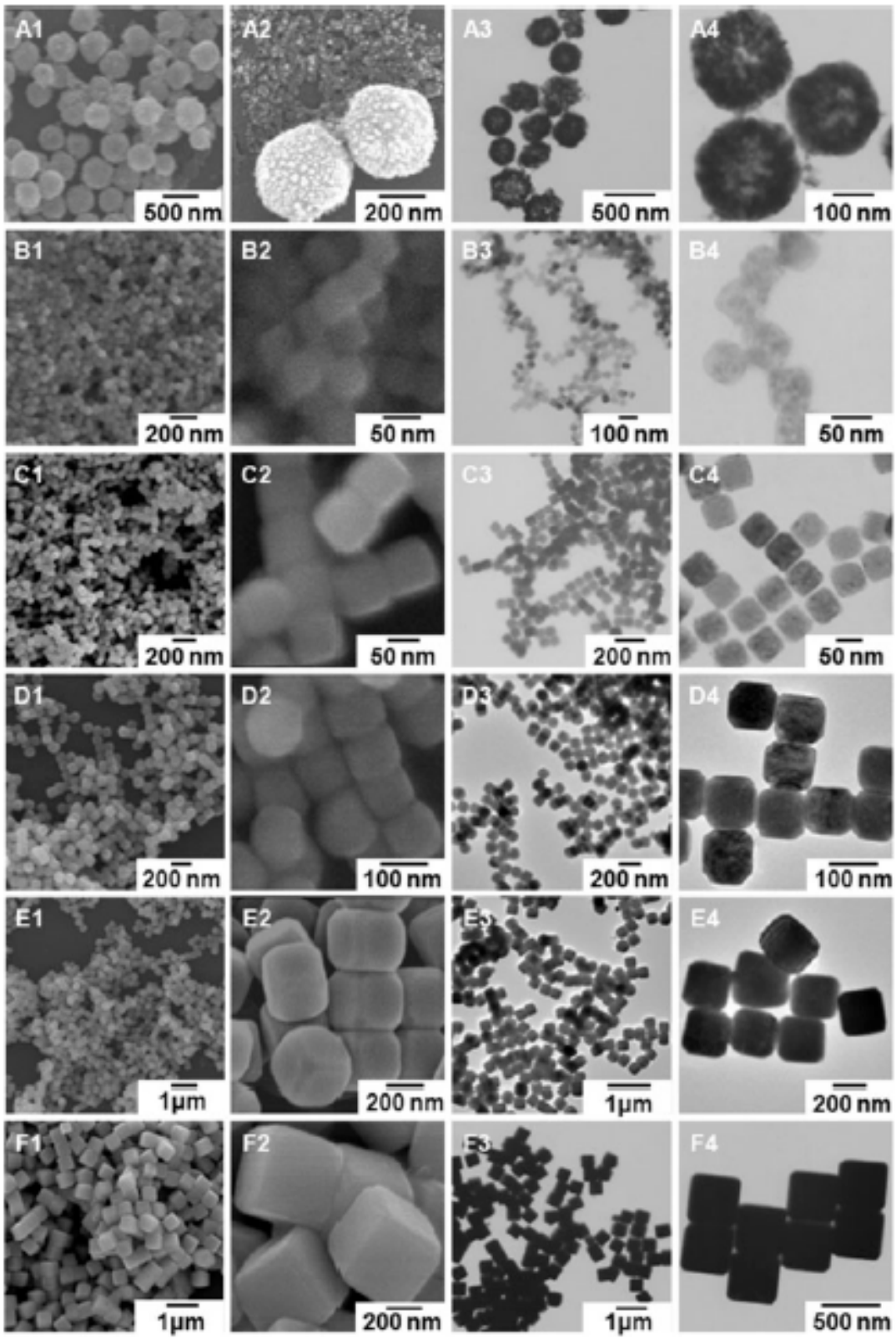

Figure 1.5. SEM (columns 1 and 2) and TEM (columns 3 and 4) images of the Cu_2O nanocubes for samples A to F (seed to transfer 5 times). [8]

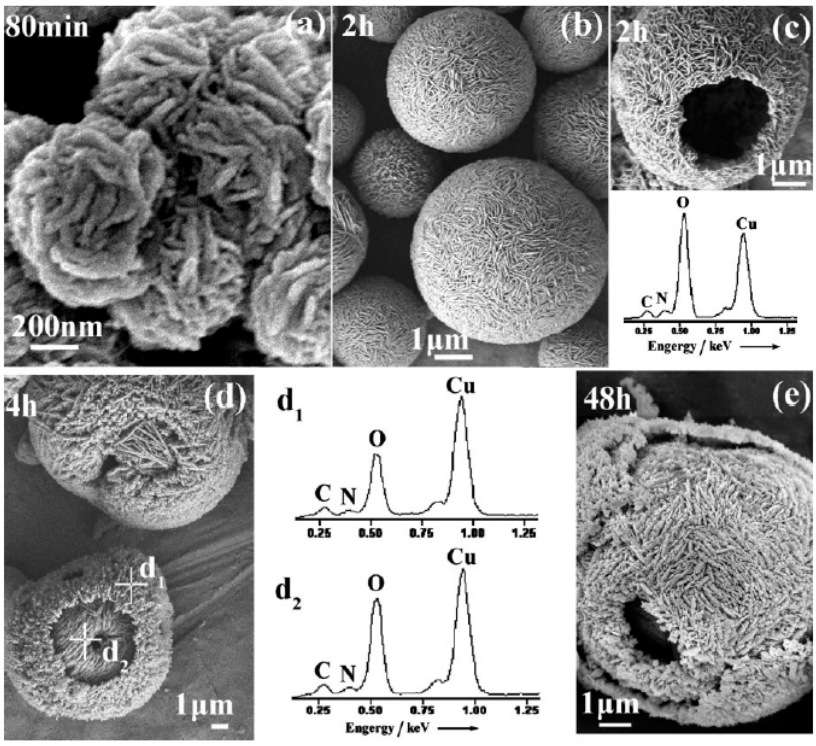

Figure 1.6. SEM images ((a) to (e)) and EDX spectra (d_1 and d_2) for the samples isolated in the time-dependent experiments with glutamic acid.[9]

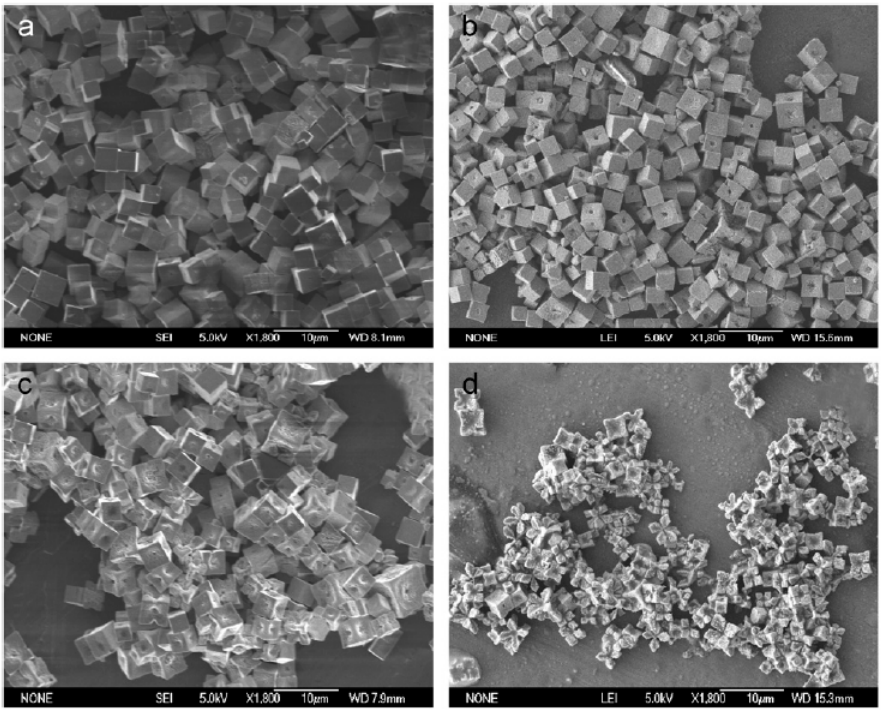

Figure 1.7. SEM images of Cu_2O particles prepared under different pH values: (a) pH of 6.5, (b) pH of 6.7, (c) pH of 7.5, and (d) pH of 8.0.[10]

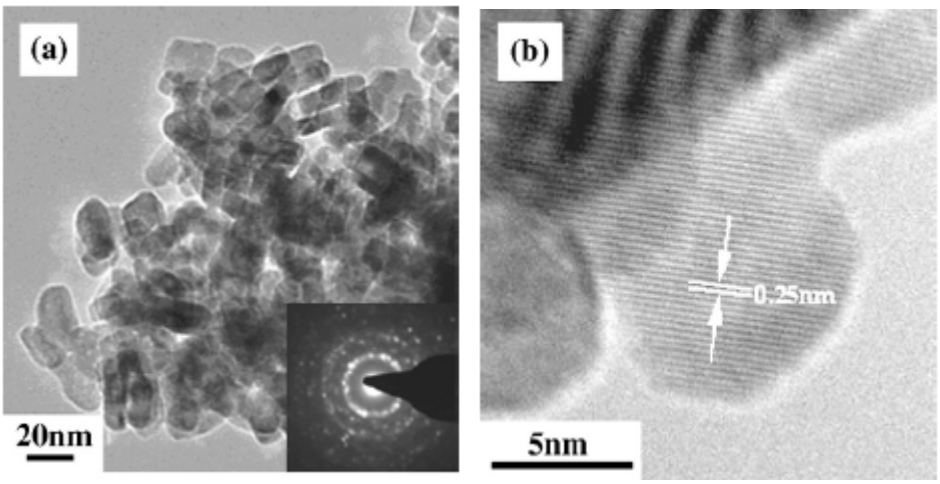

Figure 1.8. (a) TEM image (inset is the SAED patterns) and (b) HRTEM image of the Cu_2O nanorods via solvothermal treatment of $CuSO_4 \cdot 5H_2O$ and NaOH in a mixed solution of ethanol and deionized water at 140 °C for 10 hours.[11]

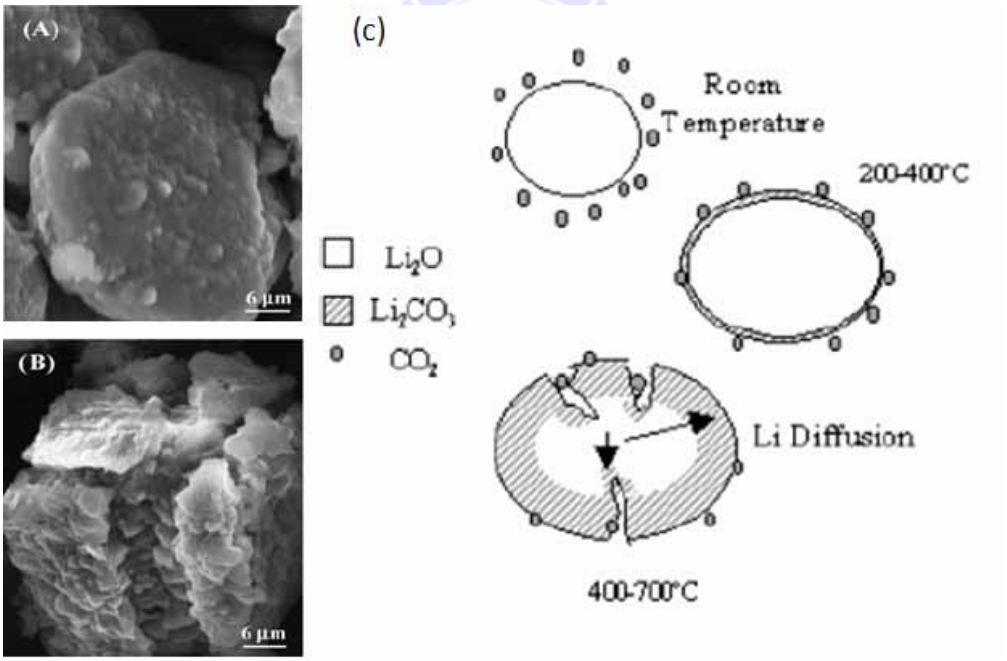

Figure 1.9. SEM image of Li_2O before treatment (A), heat treated at 600 °C for 2 hours in a CO_2 flux (B), and scheme of the mechanism proposed for CO_2 absorption on Li_2O (C).[19]

Table 1.1. Faradaic efficiencies for the products obtained in the electrochemical reduction of CO_2 at -2.4 V (Ag/AgCl) on a copper(I) halide-confined Cu-mesh electrode.[27]

Electrode system	Electrolyte (3 M)	Faradaic efficiency/%									Conver-sion/%[f]	i/mA cm^{-2}[j]
		Ethylene	Methane	CO	Ethane	Ethanol	Formic[k]	Acetic[l]	Lactic[m]	H_2		
Cu[b]	KCl	40.0	5.1	2.0	0.3	2.6	0.0	0.0	0.0	53.2	14.4	49.0–38.2
CuCl[c]	KCl	60.5	6.6	1.8	2.8	1.9	0.1	0.2	0.4	18.8	17.1	50.0–42.1
CuBr[d]	KBr	79.5	5.8	2.4	1.2	1.6	0.7	0.2	0.3	9.3	24.3	46.1–39.2
CuI[e]	KI	71.8	4.3	2.8	0.8	1.6	0.0	0.0	0.1	11.0	21.9	49.0–44.1

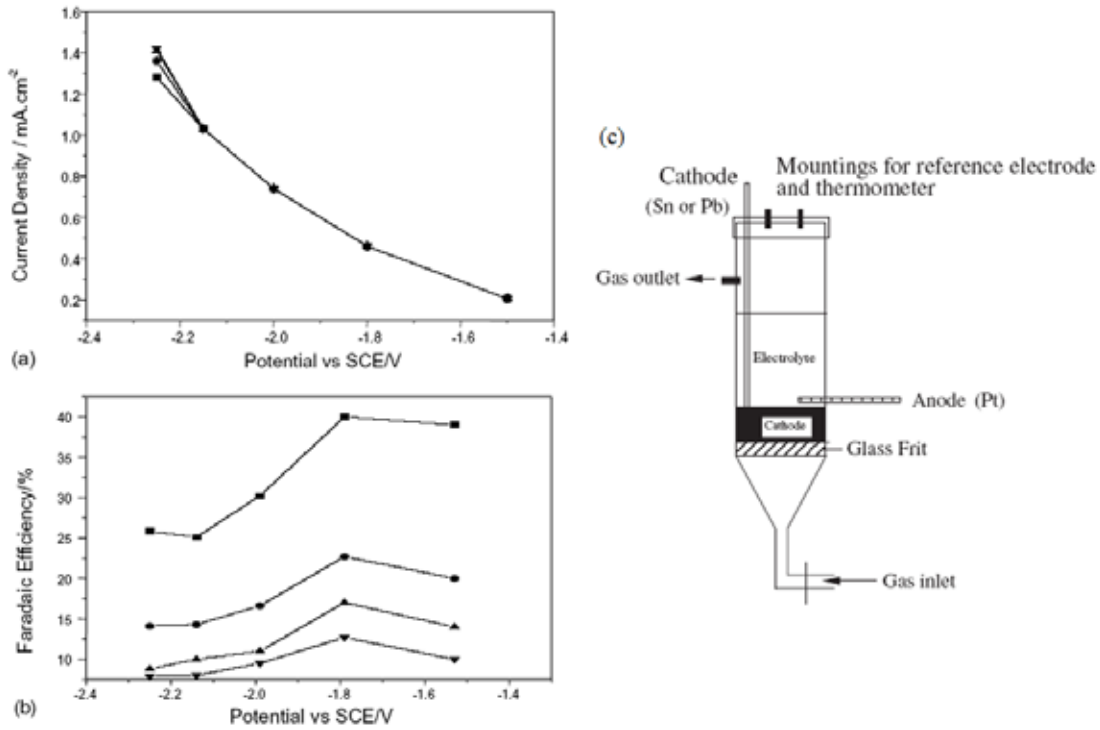

Figure 1.10. (a) The IV curves for CO_2 reduction on Pb electrode in 0.1 M K_2CO_3 at various time periods. (b) Faradaic current efficiency–potential diagram for formic acid formation on the Pb electrode in 0.1 M K_2CO_3 at different time intervals; (■) 30, (●) 60, (▲) 90, and (▼) 120 min. (c) The image of the electrochemical fixed-bed reactor.[30]

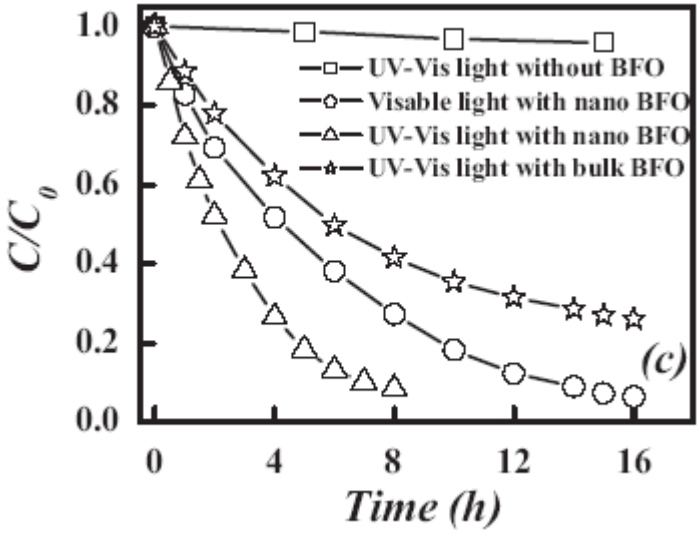

Figure 1.11. Photocatalytic ability of bulk and nanoparticulate BFO on degradation of methyl orange under irradiation of UV-vis and visible light.[34]

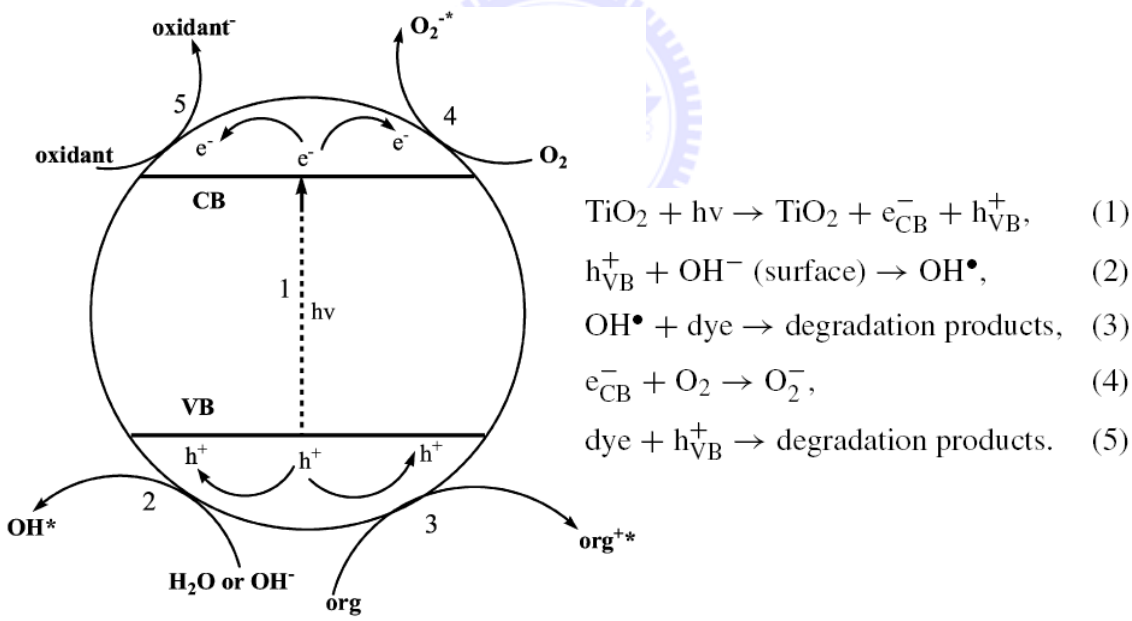

Figure 1.12. The mechanisms occurring on TiO_2 surfaces exposed to light for the photodegradation of organic pollutants.[35]

Chapter 2.
Synthesis and Characterizations of Cuprous Oxide Particles

2.1. Introduction

As the Cu_2O with various shapes and sizes demonstrates different physical properties, the formation of Cu_2O with unique morphologies has been pursued for a long time. In chapter 1, we have already provided the background information in the synthesis of Cu_2O. After careful evaluations, we selected the chemical reduction method to fabricate Cu_2O with desirable attributes.

In this research, we investigated the relations between the synthetic parameters and morphologies of the resulting powders. Our objective was to determine the critical processing conditions for specific Cu_2O and further to develop methods in effective morphologic control. We believe the results would enable us to fabricate the Cu_2O with unique structures as well as uniform sizes and shapes. Our study started with various copper(II) ion precursors in different concentrations of surfactant and sodium. Copper sulfide(II), copper(II) acetate, copper(II) nitrate, and copper(II) chloride were chosen as the copper ion sources. Polyethylene glycol with average molecular weight of 200 in different concentrations was used as the surfactant. Sodium hydroxide was used to adjust the pH value of the solution and L-ascrobic acid sodium was employed as the reducing agent. The as-synthesized Cu_2O powders were characterized by X-ray Diffraction (XRD) and Scanning

Electron Microscopy (SEM). We obtained uniform Cu_2O particles with various sizes and shapes through manipulating the synthesis parameters.

The materials and processes for the Cu_2O formation are mentioned in the experimental section (Section 2.2). The correlation between the experimental parameters and the resulting powders are discussed in section 2.3. The conclusions for this work are provided in section 2.4.

2.2. Experiment

2.2.1. Reagents

1.	$CuSO_4 \cdot 5H_2O$	Riedel-de Haën, 99 ~ 100.5 %
2.	$CuAc_2 \cdot 1H_2O$	J. T. Baker, 98.23 %
3.	$Cu(NO_3)_2 \cdot 5H_2O$	Riedel-de Haën, 98 %
4.	$CuCl_2 \cdot 5H_2O$	J. T. Baker, 99.3 %
5.	PEG (av. MW. 200)	Fluka
6.	L-ascorbic acid sodium	SIGMA
7.	NaOH	Riedel-de Haën, 99 %

2.2.2. Synthetic approaches

The starting solutions were prepared by mixing 10 mL of 0.005 M copper(II) aqueous solutions with 10.0 mL of polyethylene glycol (PEG) at various concentrations followed by shaking for 5 seconds. The concentrations for PEG were 4, 2 and, 1 M, respectively. In separate vessels, 5 mL of 0.5 M L-ascorbic acid sodium (LAAS) and 5 mL of various concentrations of NaOH

were prepared. Subsequently, the LAAS and sodium hydroxide solutions were added into the copper(II) solution with two different procedures (designed as A and B, respectively) . In procedure A, the NaOH solution was added into the solution containing copper(II) and PEG first. After 5 seconds of shaking, the LAAS was injected into the solution followed by shaking for another 5 seconds. In procedure B, the LAAS and sodium hydroxide solutions were mixed initially. Afterwards, the mixture was poured into the solution containing copper(II) and PEG. The solution was shaken for another 10 seconds. After aging for 18 hours, the Cu_2O particles precipitated at the bottom of the vessels with their color appearing in different colors. The precipitates were collected by removing the supernatant liquid. The obtained Cu_2O particles were re-dispersed in water and another supernatant liquid removing process was used as soon as the Cu_2O particles re-precipitated at the bottom of the vessels. Through these processes we fabricated pure Cu_2O particles without surfactant.

We also adopted the Taguchi Method to find the relation between the products and the experimental parameters. A set of solutions was prepared by mixing 10 mL of 0.005 M copper(II) solutions with 10.0 mL PEG at various concentrations. The concentrations of PEG are 2, 0.2, 0.02, and 0.002 M, respectively. After shaking for 5 seconds, we added NaOH solution with a variety of concentrations from 2 to 0.002 M to the solution containing copper(II) and PEG. The mixture was also shaken for 5 seconds and 0.05 M LAAS was injected into the mixture. After 10 seconds of shaking, the whole solutions were aged for 6 hours to obtain the Cu_2O particles precipitating at the bottom of the vessels. The precipitates were collected by removing the supernatant liquid. The obtained Cu_2O particles were re-dispersed in water

and another supernatant liquid removing process was employed as soon as the Cu_2O particles re-precipitated at the bottom of the vessels. Through these processes we fabricated pure Cu_2O particles without any precursors.

2.2.3. Materials Characterizations

A. High Resolution X-ray Diffractometer (XRD)

To determinate their crystal structures, the obtained Cu_2O particles were characterized by X-ray diffraction (XRD) using a Bedi D1 diffractometer with Cu Kα radiation in a Bragg-Brentano geometry.

B. Scanning Electron Microscopy (SEM)

The SEM images for the Cu_2O particles were taken by a Hitachi JSM 6700F. The samples were prepared by spreading the powders onto a carbon substrate on the sample holder followed by a conductivity improvement step by Pt deposition.

2.3. Results and Discussion

In this section, we discuss the influence of the experimental parameters such as copper(II) ion sources, surfactant concentration, base concentration, and synthetic method on the growth of Cu_2O particles.

2.3.1. Characterization on the synthesized Cu_2O particles

After altering the relevant experimental parameters we obtained the Cu_2O powders with four different colors. The XRD was used to identify their respective phases and the results indicated pure Cu_2O phases were present for all samples. The most intense XRD peak for the Cu_2O powder was the (111) peak followed by the (200), (220), and (311).

The (111) peak was located at 2 theta of 36.4°, the (200) peak was positioned at 2 theta of 42.4°, the (220) peak was located at 2 theta of 61.4°, and (311) peak was located at 2 theta of 73.6°. The (110) peak, which was almost buried in the noises, was located at 2 theta of 29.6°. Figure 2.3 exhibits the XRD data.

We determine the colors of the Cu_2O particles corresponding to various sizes and shapes by SEM images. The Cu_2O particles with diameters larger than 1 μm exhibit red color. The Cu_2O cubes with diameters from 300 to 1000 nm appeared in orange color. The Cu_2O cubes with diameters from 100 to 300 nm revealed yellow color. The disordered Cu_2O particles with diameter less than 300 nm were brown color.

2.3.2. The influence of surfactant concentration on the Cu_2O growth

Surfactants are typically organic compounds containing hydrophobic and hydrophilic groups to reduce the interfacial tension between water and oil. As a general rule, one expects that as the concentration of the surfactant (capping agent) increases, the resulting particle size would be decreased. It is because that the sites for further nucleation and growth are blocked by the

capping agent.

We adjusted the concentration of PEG from 0.002 to 2 M in order to explore the relationship between the particle sizes and surfactant concentrations. The SEM images (figure 2.4) confirmed the results that the morphologies of the Cu_2O particles revealed negligible change when we used $CuCl_2$ as the copper(II) ion source. In contrast, when we used $CuAc_2$ or $Cu(NO_3)_2$ as the copper(II) ion source, 2 M PEG led to the smallest Cu_2O particles and the other concentrations of PEG produced Cu_2O particles with identical sizes.

2.3.3. The influence of base concentration on the Cu_2O growth

To attain the relation between base concentration and Cu_2O particle sizes we controlled the concentration of the NaOH solution from 0.002 to 2 M. Decreasing the concentration of base from 2 to 0.02 M we obtained the Cu_2O particles with diameters varying from 1570 to 170 nm. However, when we reduced the concentration of NaOH further from 0.02 to 0.002 M, the Cu_2O particles changed their shapes from uniform cubes to irregular spheres.

In thermodynamics, the Pourbaix diagram (figure 2.5) provides the equilibrium phase of a material at various pH and potentials. Through Pourbaix diagram we knew the states of copper ions at equilibrium and possibly their effects on subsequent Cu_2O growth. There were other ions such as Cl^-, SO_4^{2-}, NO_3^-, and CH_3COO^- in the solution which may affect the states of copper ions at equilibrium, but the concentration for those ions were too small to influence the equilibrium states.

With addition of 2 M NaOH into the solution including copper(II) and PEG, the pH value of the solution was increased over 13 and the solution

became blue, which meant copper(II) existed as CuO_2^{2-}. The CuO_2^{2-} in the solution was likely to be surrounded by Na^+. Thus the copper ions used to grow the Cu_2O were released slowly and the Cu_2O particles were found to grow gradually. From the SEM pictures at pH of 13 the Cu_2O particles was approximately 1500 nm.

When 0.2 M PEG was added into the solution including copper(II) and PEG, the pH of the solution was increased to 12 to produce $Cu(OH)_2$, which exhibited blue and small particles suspended in the solution (However, it is to be noted that the observation were inconsistent with the Pourbaix diagram.) The suspended blue particles disappeared instantly when the LAAS was added and the solution changed its color from light blue to orange. The SEM pictures presented that the particle size of Cu_2O particles growth at pH of 12 is about 700 nm.

Adding 0.02 M NaOH into the solution including copper(II) and PEG, the pH value was 11 and the copper(II) in the solution also became $Cu(OH)_2$. When the LAAS was added into the light blue solution containing suspended $Cu(OH)_2$, the small Cu_2O particles appeared with yellow color, changing the solution color from blue to yellow. The particle size of Cu_2O growth at pH of 11 was smaller than that of pH of 12. It may result from the particle size of the $Cu(OH)_2$. We found out that the $Cu(OH)_2$ particles formed in the pH of 12 solution precipitated faster than the particles formed in the pH of 11 solution (shown in figure 2.6). We believe that the particle size of Cu_2O at different pH changed significantly since the copper(II) exists in various forms at different pH values.

2.3.4. The influence of synthetic method on the Cu_2O growth

We used two methods (method A and B) in preparing the Cu_2O particles to study the relationship between the synthetic method and morphologies of Cu_2O particles. In procedure A, the NaOH and the LAAS were added into the solution containing copper(II) sources and PEG. In this way we prepared the Cu_2O particles with base concentrations from 0.002 to 2 M. On the other hand, when procedure B (NaOH and LAAS were mixed and injected into the solution containing copper(II) sources and PEG) was used to prepare the Cu_2O particles, the base concentration was higher than 0.2 M. If the base concentration was lower than 0.2 M, the Cu_2O particles could not be formed ever after aging for 6 hours.

Through SEM pictures we determined that procedure B was able to produce smaller Cu_2O particles than procedure A under identical conditions. We surmise that differences of copper(II) sources in the solutions were responsible. The copper ion sources for procedure A were CuO_2^{2-} and $Cu(OH)_2$ when the base concentrations were 2 and 0.2 M. In contrast, the copper ion sources for procedure B were copper(II) when the base concentrations were 2 and 0.2 M.

2.4. Conclusions

After careful analysis of our data, we come to several conclusions. First, changing the concentration of the surfactant (PEG) plays negligible influence over the particle sizes of the Cu_2O. Second, the adding sequence of NaOH and LAAS influences the morphologies of the resulting Cu_2O particles. When

the NaOH was added to the solution containing copper(II) before LAAS, the obtained Cu_2O particles were bigger than the particles obtained from adding NaOH and LAAS simultaneously. Third, adjusting the pH value of the solution leads to distinct particle sizes, a fact from the differences of copper ion sources. Lastly, we have succeeded in synthesizing the Cu_2O cubes with tunable edge length from 1570 to 170 nm through varying the NaOH concentrations of the solutions from 2 to 0.02 M.

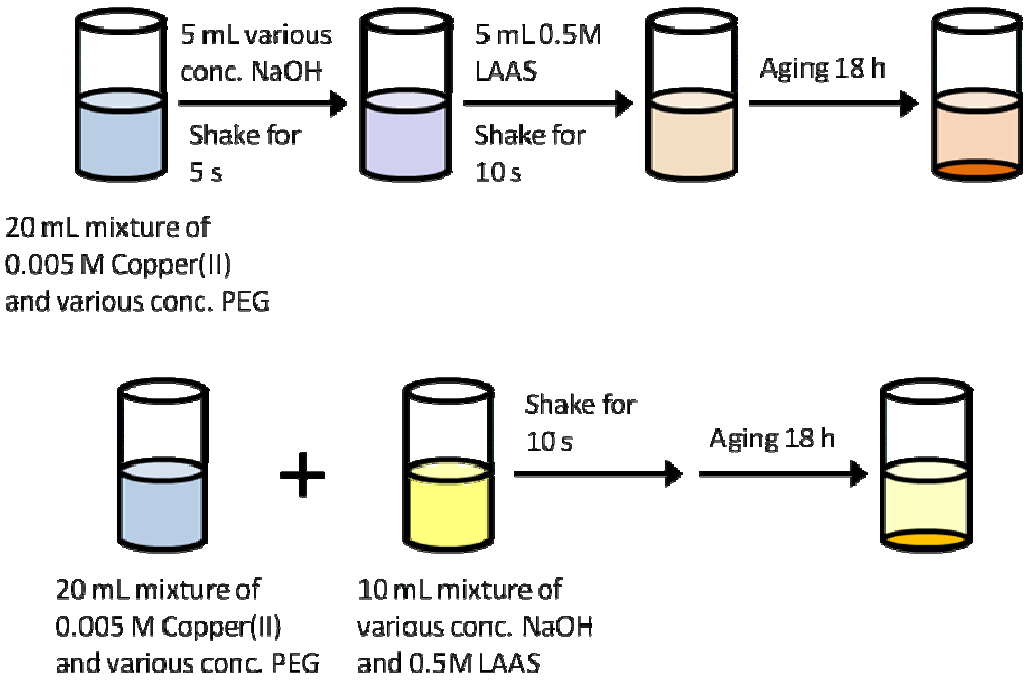

Figure 2.1. Illustration of procedure A (above) and B (below), used to grow Cu_2O particles.

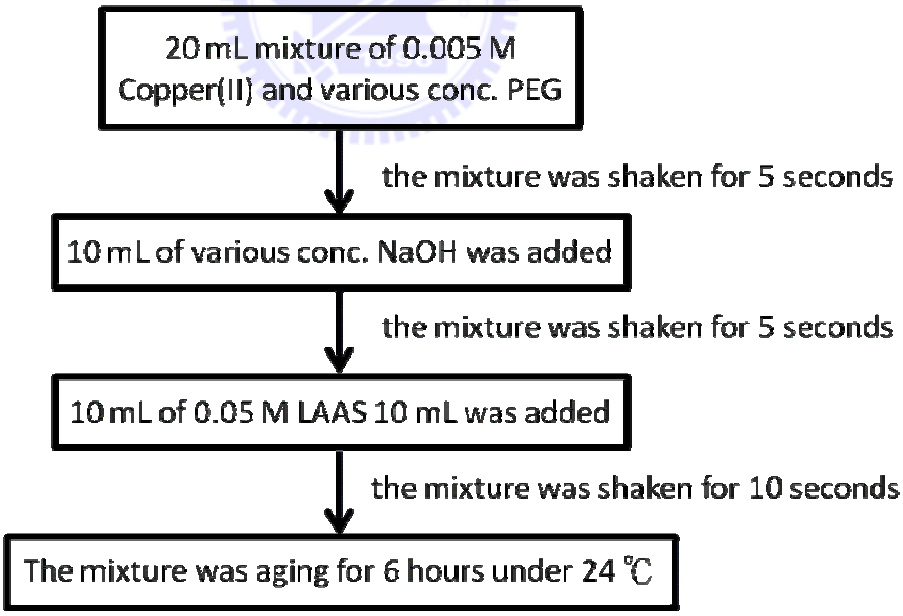

Figure 2.2. Illustration of synthetic process of Cu_2O particles.

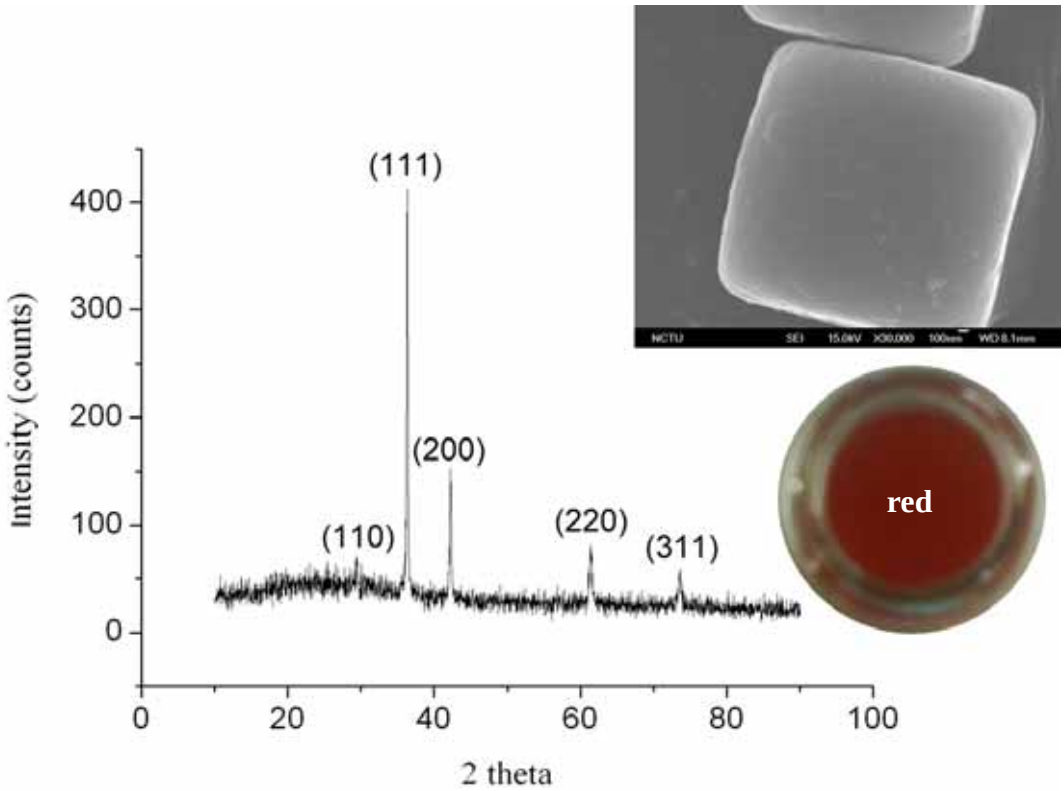
(111)
(200)
(110)
(220)
(311)
Intensity (counts)
2 theta
red

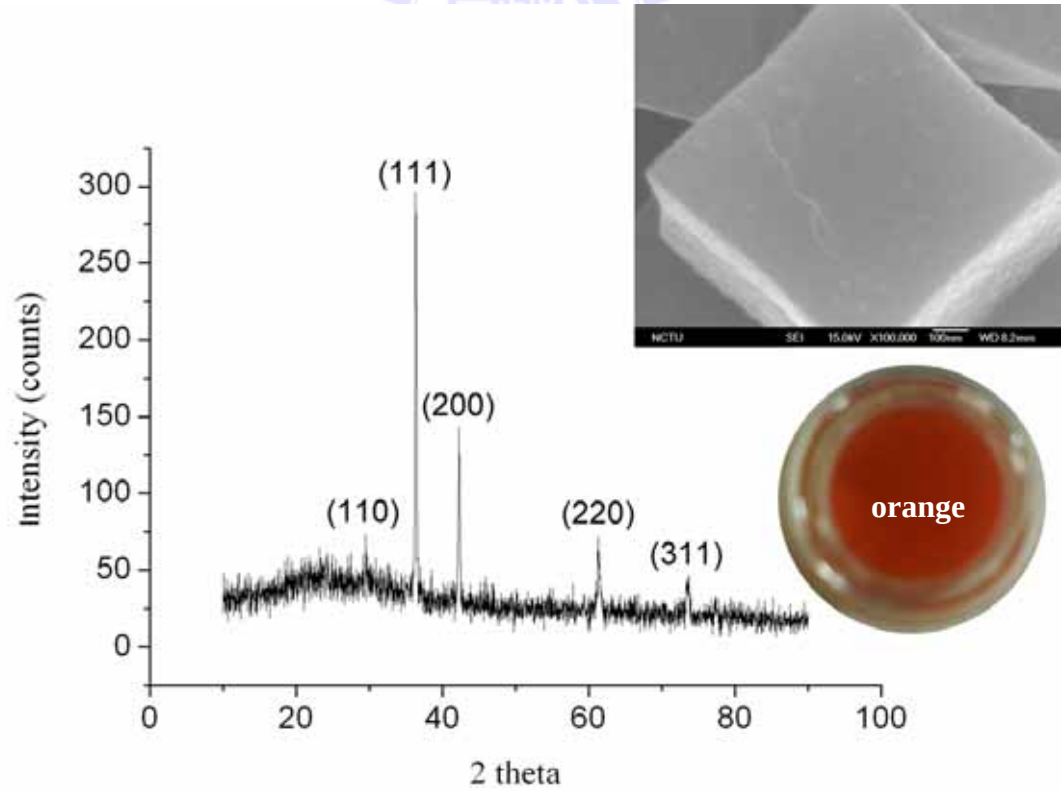
(111)
(200)
(110)
(220)
(311)
Intensity (counts)
2 theta
orange

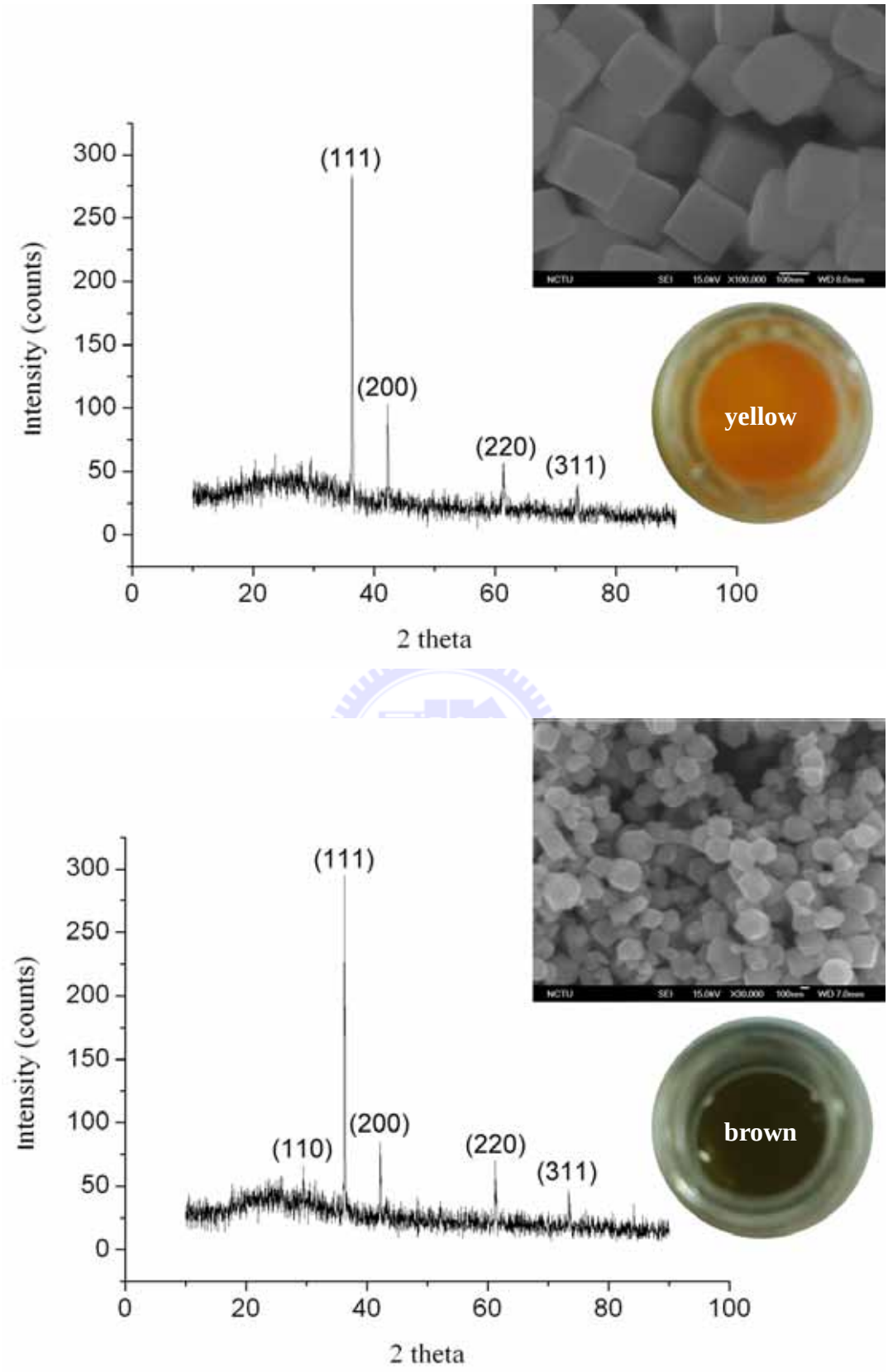

Figure 2.3. Four different sizes of Cu_2O particles with four different colors.

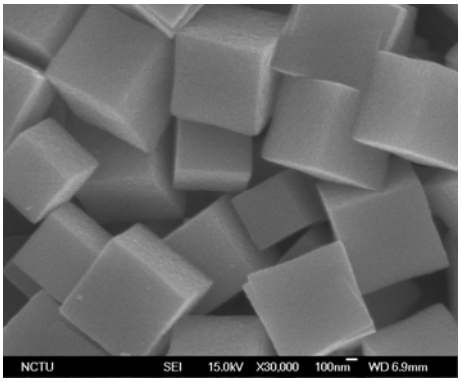

Method A and aging for 6 hours

$CuCl_2$ (0.005 M), **PEG (200) (2 M)**,

NaOH (0.2 M), and LAAS (0.05 M)

Particle size: 647 nm

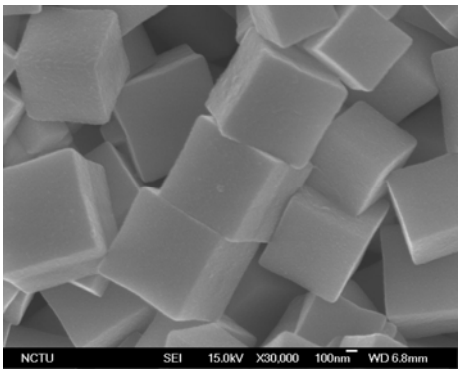

Method A and aging for 6 hours

$CuCl_2$ (0.005 M), **PEG (200) (0.2 M)**,

NaOH (0.2 M), and LAAS (0.05 M)

Particle size: 642 nm

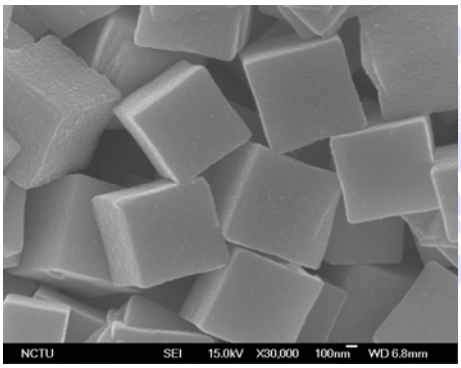

Method A and aging for 6 hours

$CuCl_2$ (0.005 M), **PEG (200) (0.02 M)**,

NaOH (0.2 M), and LAAS (0.05 M)

Particle size: 661 nm

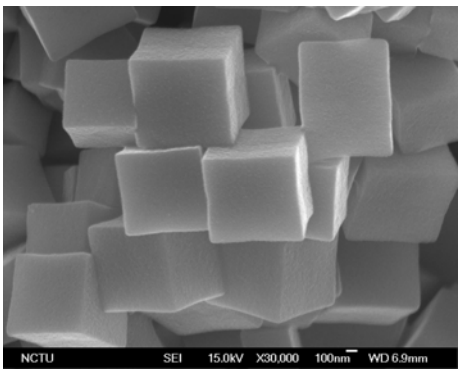

Method A and aging for 6 hours

$CuCl_2$ (0.005 M), **PEG (200) (0.002 M)**,

NaOH (0.2 M), and LAAS (0.05 M)

Particle size: 655 nm

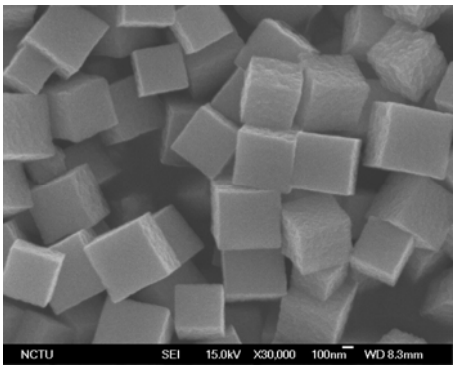

Method A and aging for 6 hours

$CuAc_2$ (0.005 M), **PEG (200) (2 M)**,

NaOH (0.2 M), and LAAS (0.05 M)

Particle size: 430 nm

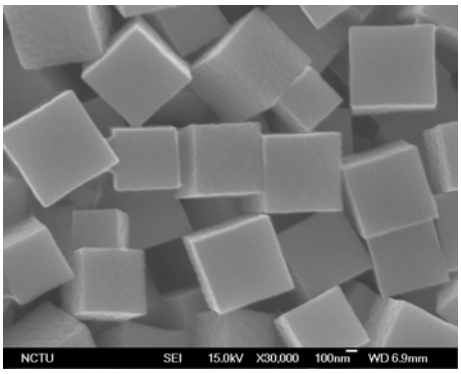

Method A and aging for 6 hours

$CuAc_2$ (0.005 M), **PEG (200) (0.2 M)**,

NaOH (0.2 M), and LAAS (0.05 M)

Particle size: 522 nm

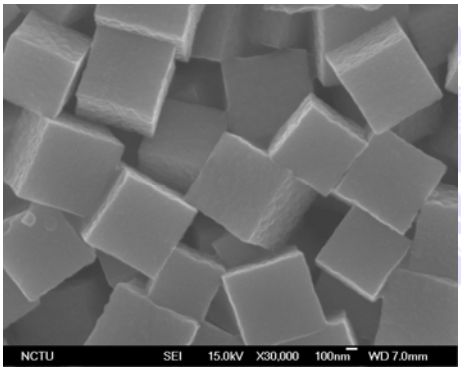

Method A and aging for 6 hours

$CuAc_2$ (0.005 M), **PEG (200) (0.02 M)**,

NaOH (0.2 M), and LAAS (0.05 M)

Particle size: 605 nm

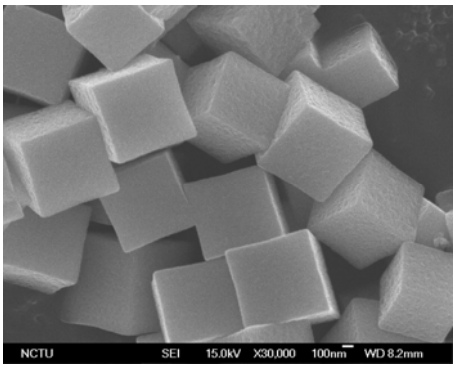

Method A and aging for 6 hours

$CuAc_2$ (0.005 M), **PEG (200) (0.002 M)**,

NaOH (0.2 M), and LAAS (0.05 M)

Particle size: 598 nm

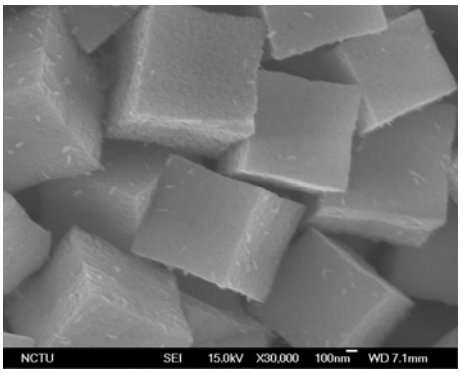

Method A and aging for 6 hours

$Cu(NO_3)_2$ (0.005 M), **PEG (200) (2 M)**, NaOH (0.2 M), and LAAS (0.05 M)

Particle size: 927 nm

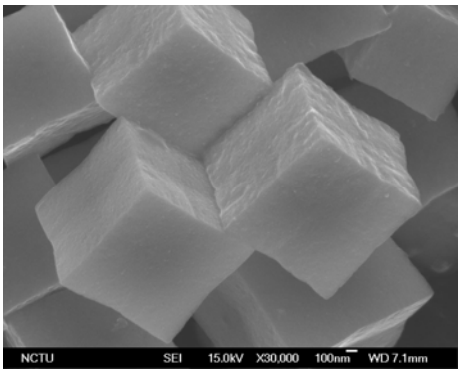

Method A and aging for 6 hours

$Cu(NO_3)_2$ (0.005 M), **PEG (200) (0.2 M)**, NaOH (0.2 M), and LAAS (0.05 M)

Particle size: 1109 nm

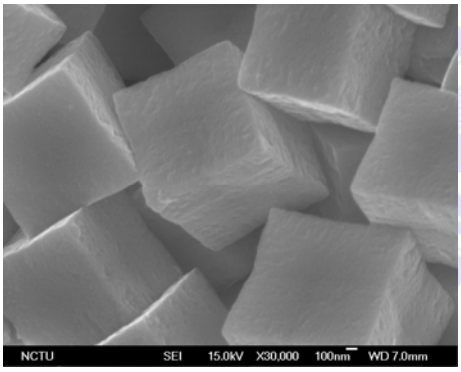

Method A and aging for 6 hours

$Cu(NO_3)_2$ (0.005 M), **PEG (200) (0.02 M)**, NaOH (0.2 M), and LAAS (0.05 M)

Particle size: 1092 nm

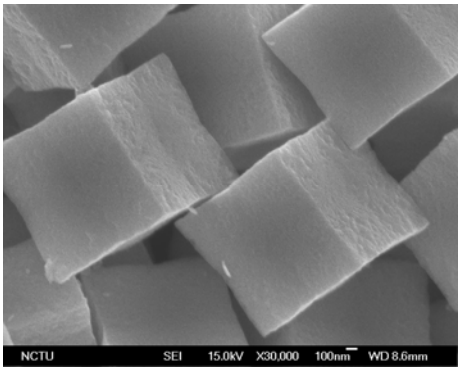

Method A and aging for 6 hours

$Cu(NO_3)_2$ (0.005 M), **PEG (200) (0.002 M)**, NaOH (0.2 M), and LAAS (0.05 M)

Particle size: 1121 nm

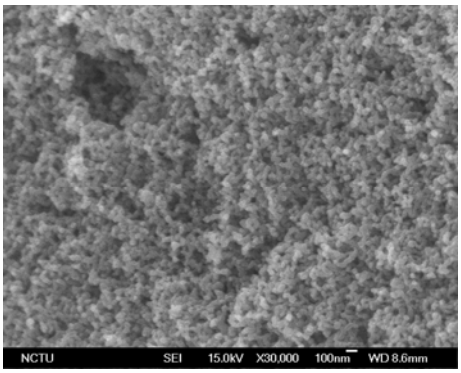

Method A and aging for 6 hours

$CuCl_2$ (0.005 M), **PEG (200) (2 M)**,

NaOH (0.2 M), and LAAS (0.05 M)

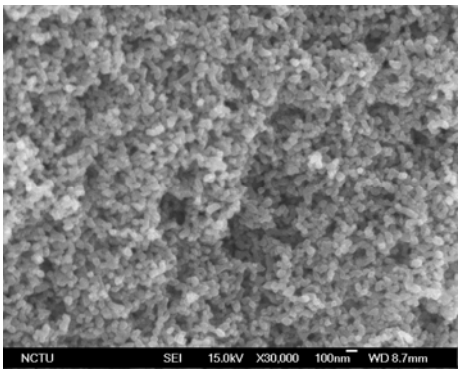

Method A and aging for 6 hours

$CuCl_2$ (0.005 M), **PEG (200) (0.2 M)**,

NaOH (0.2 M), and LAAS (0.05 M)

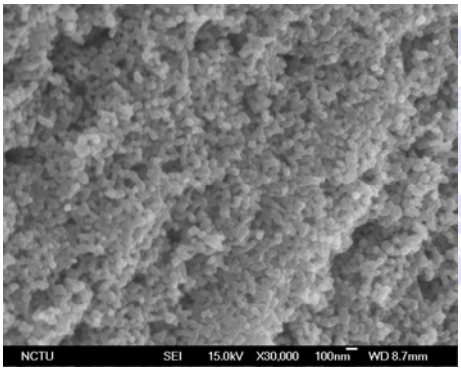

Method A and aging for 6 hours

$CuCl_2$ (0.005 M), **PEG (200) (0.02 M)**,

NaOH (0.2 M), and LAAS (0.05 M)

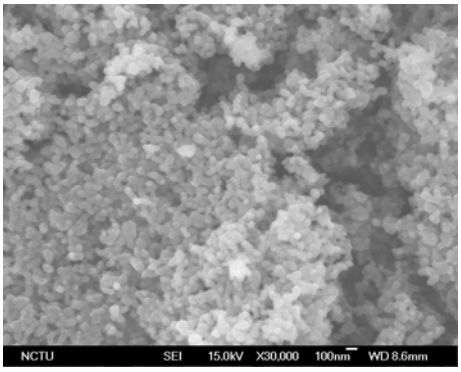

Method A and aging for 6 hours

$CuCl_2$ (0.005 M), **PEG (200) (0.002 M)**,

NaOH (0.2 M), and LAAS (0.05 M)

Figure 2.4. SEM images of Cu_2O particles synthesized through different concentrations of PEG (200).

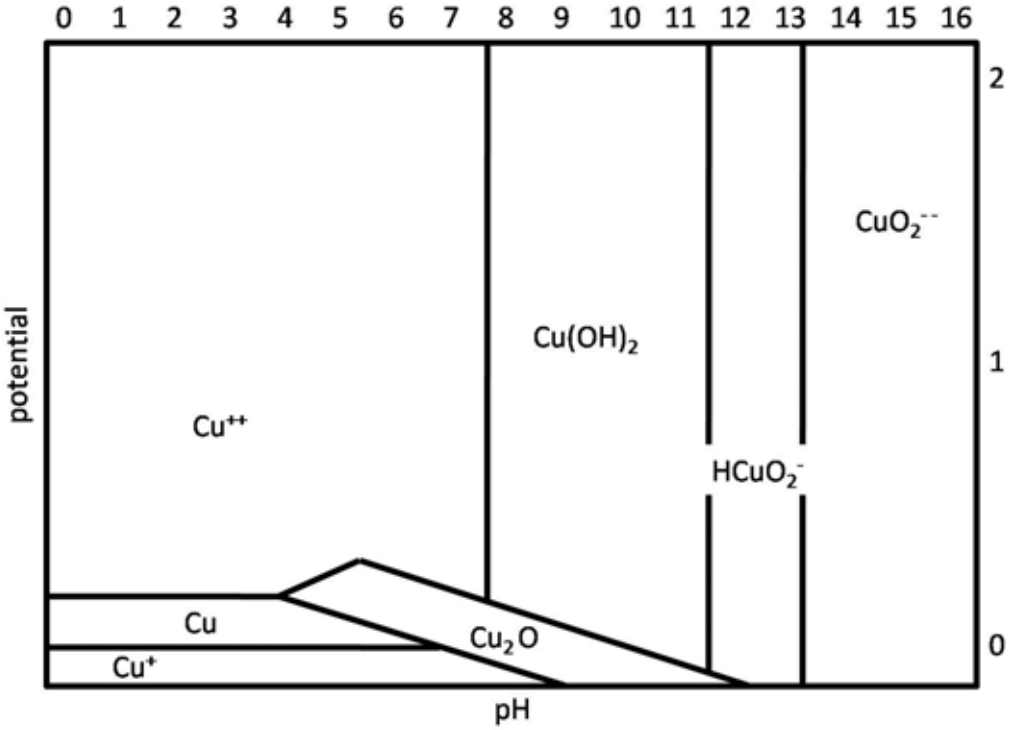

Figure 2.5. Part of the Pourbaix diagram for the Cu in different potentials and pH.

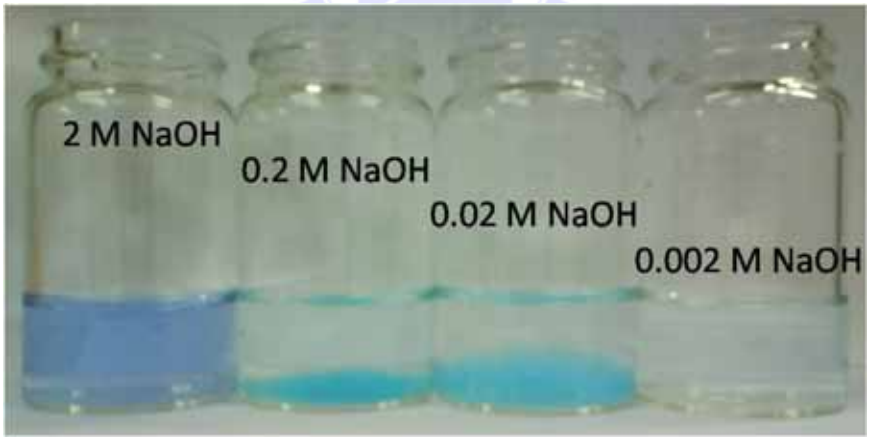

Figure 2.6. The color of the solution after adding 10 mL of various concentrations of NaOH into the solution containing copper(II) and PEG.

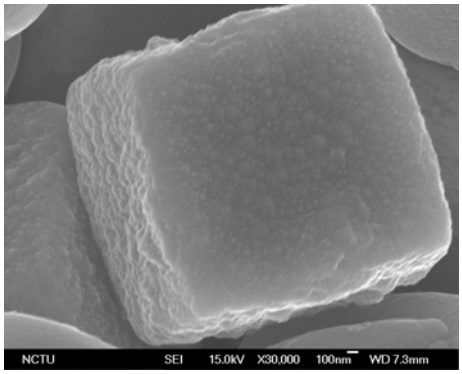

Method A and aging for 6 hours

$Cu(NO_3)_2$ (0.005 M), PEG (200) (0.2 M),

NaOH (2 M), and LAAS (0.05 M)

Particle size: 2513 nm

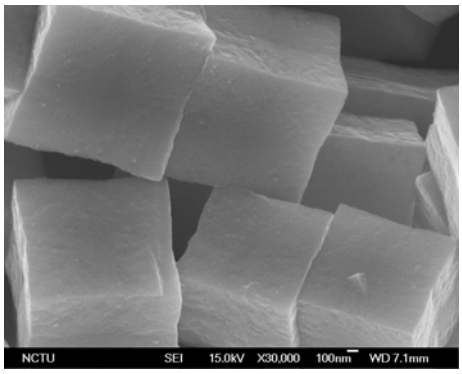

Method A and aging for 6 hours

$Cu(NO_3)_2$ (0.005 M), PEG (200) (0.2 M),

NaOH (0.2 M), and LAAS (0.05 M)

Particle size: 1109 nm

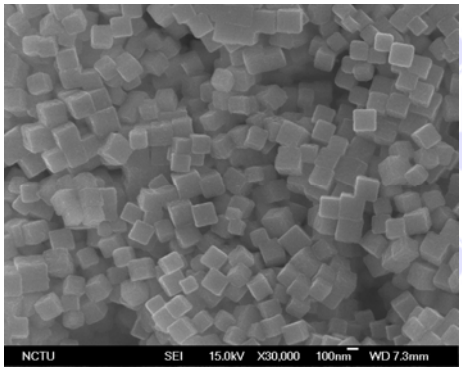

Method A and aging for 6 hours

$Cu(NO_3)_2$ (0.005 M), PEG (200) (0.2 M),

NaOH (0.02 M), and LAAS (0.05 M)

Particle size: 167 nm

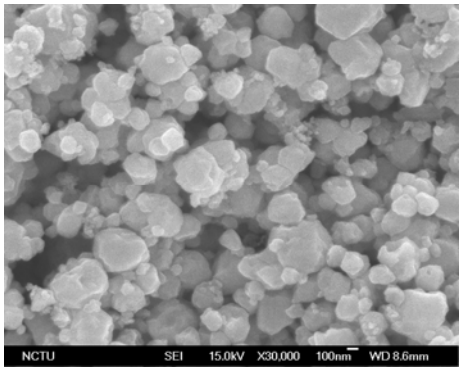

Method A and aging for 6 hours

$Cu(NO_3)_2$ (0.005 M), PEG (200) (0.2 M),

NaOH (0.002 M), and LAAS (0.05 M)

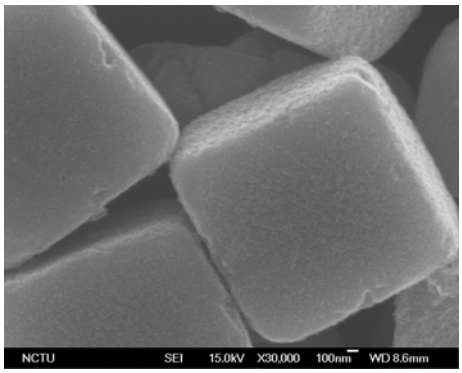

Method A and aging for 6 hours

$CuSO_4$ (0.005 M), PEG (200) (0.2 M),

NaOH (2 M), and LAAS (0.05 M)

Particle size: 1273 nm

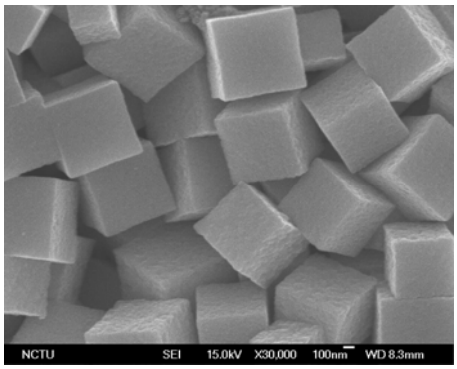

Method A and aging for 6 hours

$CuSO_4$ (0.005 M), PEG (200) (0.2 M),

NaOH (0.2 M), and LAAS (0.05 M)

Particle size: 582 nm

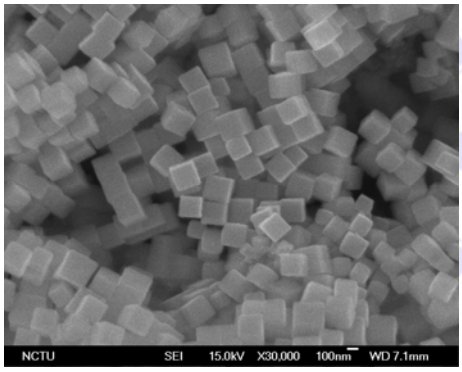

Method A and aging for 6 hours

$CuSO_4$ (0.005 M), PEG (200) (0.2 M),

NaOH (0.02 M), and LAAS (0.05 M)

Particle size: 188 nm

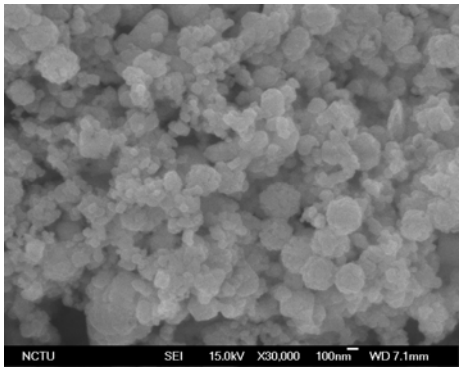

Method A and aging for 6 hours

$CuSO_4$ (0.005 M), PEG (200) (0.2 M),

NaOH (0.002 M), and LAAS (0.05 M)

Figure 2.7. SEM images of the Cu_2O particles synthesized at different pH values of the solution.

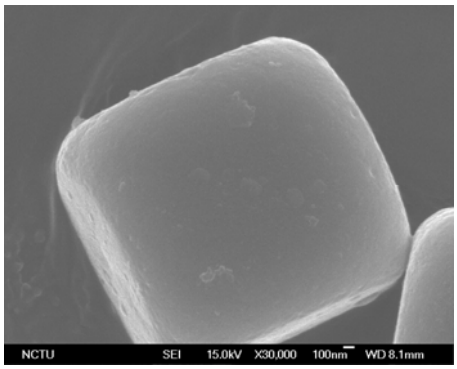

Method A and aging for 6 hours

$CuCl_2$ (0.005 M), PEG (200) (2 M),

NaOH (2 M), and LAAS (0.05 M)

Particle size: 1776 nm

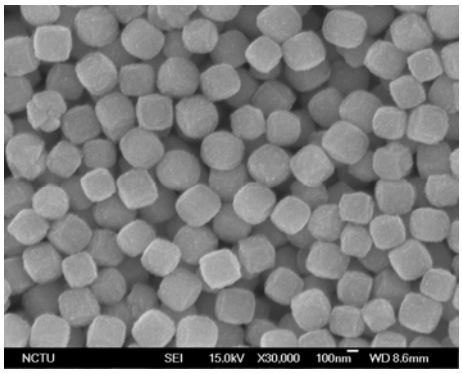

Method B and aging for 6 hours

$CuCl_2$ (0.005 M), PEG (200) (2 M),

NaOH (2 M), and LAAS (0.05 M)

Particle size: 347 nm

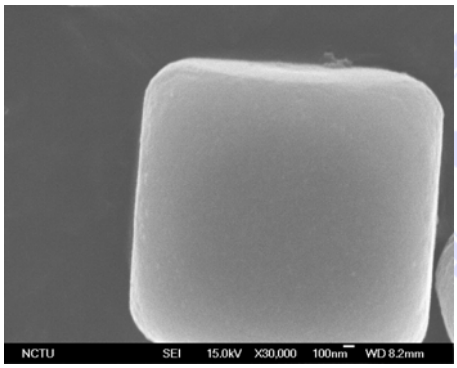

Method A and aging for 6 hours

$CuCl_2$ (0.005 M), PEG (200) (0.002 M),

NaOH (2 M), and LAAS (0.05 M)

Particle size: 1699 nm

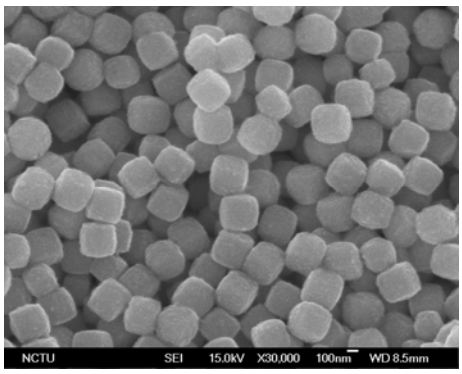

Method B and aging for 6 hours

$CuCl_2$ (0.005 M), PEG (200) (0.002 M),

NaOH (2 M), and LAAS (0.05 M)

Particle size: 352 nm

Figure 2.8. SEM images of the Cu_2O particles synthesized through different methods.

Chapter 3.

Electrochemical Reduction of Carbon Dioxide with Gas Diffusion Electrodes Catalyzed by Cuprous Oxide

3.1. Introduction

Reducing the CO_2 atmospheric concentration has become a popular subject since the CO_2 is recognized as one of the primary greenhouse gases that contributes to the rising temperature. Previously in chapter 1, we mentioned how the other researchers explored practical methods to reduce the CO_2 concentration in the atmosphere. In our lab, we adopted the electrochemical reduction method to investigate possible CO_2 reduction by gas diffusion electrodes catalyzed by Cu_2O particles.

In this chapter, we report our progress over the influences of the electrolytes and catalysts on the CO_2 reducing abilities for the gas diffusion electrodes catalyzed by the Cu_2O. Our objective was to determine whether the Cu_2O could be a desirable catalyst for electrochemical reduction of CO_2. Furthermore, we intended to identify the optimized parameters for CO_2 reduction. Three different sizes of Cu_2O particles with diameters of 1570, 640, and 170 nm were chosen as the catalysts depositing on the gas diffusion electrodes. $NaHCO_3$, NaOH, and $CaCl_2$ were used as the electrolytes. The performances for electrochemical reduction performances were analyzed by a potentiostat. Among those electrodes, we obtained the best result when the

NaOH was used with the Cu_2O particles in diameter of 640 nm.

The electrochemical setup, fabrication of gas diffusion electrode, and electrochemical analysis are mentioned in the experimental section (Section 3.2). The correlation between the experimental parameters and electrochemical performances for the electrolytes and catalysts are discussed in section 3.3. The conclusions for this work are provided in section 3.4.

3.2. Experimental

3.2.1. Electrochemical setup

An unique electrolysis cell (shown in figure 3.1.) was designed for electrochemical reduction of CO_2 and we employed a potentiostat model 263A from Princeton Applied Research to characterize the performance of the gas diffusion electrode. The electrolysis cell consisted of a glass container with an electrolyte volume about 600 mL. The Pt plate with a surface area about 8 cm^2 was used as the counter electrode and saturated calomel electrode (SCE) was used as the reference electrode. The working area for the working electrode was 2.835 cm^2.

3.2.2. Fabrication of gas diffusion electrode

A. <u>Reagents</u>

1. Ethanol DuPont, 99.5 vol%

2. Nafion solution Grand Hand Instrument Co., LTD., 5 wt%
3. Hydrophobic carbon clothes Chung- Shan Institute of Science and Technology (CSIST)
4 $NaHCO_3$ J. T. Baker, 100.1 %
5 NaOH Riedel-de Haën, 99 %
6 $CaCl_2$ J. T. Baker
7. As-prepared Cu_2O particles with a diameter of 1570 nm

   Method: method A and aging for 6 hours

   Reagents: $CuCl_2$ (0.005 M), PEG (200) (2 M), NaOH (2 M), and LAAS (0.05 M)

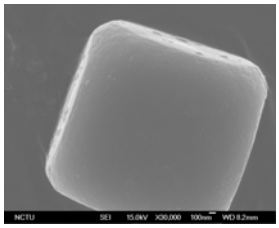

8. As-prepared Cu_2O particles with a diameter of 640 nm

   Method: method A and aging for 6 hours

   Reagents: $CuCl_2$ (0.005 M), PEG (200) (0.002 M), NaOH (0.2 M), and LAAS (0.05 M)

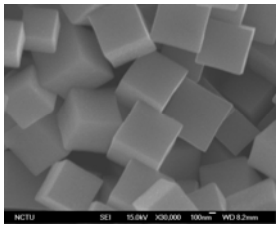

9. As-prepared Cu_2O particles with a diameter of 170 nm

   Method: method A and aging 6 hours

   Reagents: $CuCl_2$ (0.005 M), PEG (200) (0.002 M), NaOH (0.2 M), and LAAS (0.05 M)

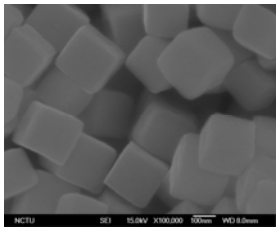

B. Fabrication process

To fabricate the gas diffusion electrodes we mixed the as-prepared Cu_2O particles, 5 wt% Nafion solution, and 99.5 vol% ethanol together.

After 10 min of ultrasonication, we dropped the mixture on the carbon clothes with a surface area about 7.5 cm^2. The carbon clothes were transferred to the hot plate to evaporate the ethanol from the mixture. Once the ethanol was removed, the process was repeated multiple times to acquire desirable catalyst loading of 1 $mgcm^{-2}$. Figure 3.2 depicts the illustration of steps involved in gas diffusion electrode fabrications.

3.2.3. Electrochemical analysis

In order to investigate the performances of Cu_2O on the electrochemical reduction of CO_2 we adopted the Cu_2O particles in three different morphologies. The photographs and SEM images of the Cu_2O catalyzed gas diffusion electrodes are presented in figure 3.3 and 3.4. In addition, three different aqueous electrolytes (0.5 M), including NaOH, $NaHCO_3$, and $CaCl_2$ were explored as well. They were arranged in a three electrode cell and where 500 mL of 0.5 M electrolyte was poured into the electrolysis cell. The CO_2 gas was bubbled into the electrolyte for 10 min at a rate of 1 $mLmin^{-1}$ prior to the experiment.

The cyclic voltammetry analysis was performed in a range from 0 to -1.705 V (vs. SCE) under constant CO_2 gas flowing. In control experiment, we analyzed the cyclic voltammetry performance of N_2 gas under identical setups.

We employed the potentiostatic method to obtain the stability of the electrochemical performances. The CO_2 gas was bubbled into the electrolyte for 10 min at a rate of 1 $mLmin^{-1}$ before electrolysis. The potentiostatic analysis was performed at a voltage of 1.705 V (vs. SCE) under the CO_2 gas

flowing into the electrolyte with a flow rate of 1 $mLmin^{-1}$. Figure 3.5 presents the illustration of electrochemical analysis.

3.3. Results and discussion

To determine the highest electrochemical reduction of CO_2 among three different electrolytes and Cu_2O particles in three different morphologies, we analyzed the electrochemical performances by cyclic voltammetry and potentiostatic method.

3.3.1. Results from cyclic voltammetry

A. The influence of three different electrolytes on the electrochemical reaction of CO_2

Figure 3.6 exhibits the current-potential curves with the Cu_2O particles (diameter of 1570 nm) catalyzed gas diffusion electrode in three different electrolytes under N_2 gas flowing. The current density from these three electrolytes at the potential of -1.7 V revealed substantial differences. The electrolyte of NaOH presented the highest current density of -15 $mAcm^{-2}$, while the electrolyte of $CaCl_2$ showed a current density of -8.82 $mAcm^{-2}$. In contrast, the electrolyte of $NaHCO_3$ exhibited the lowest current density of -4.6 $mAcm^{-2}$. The current-potential curves in figure 3.7 were the electrochemical performances of the Cu_2O particles (diameter of 1570 nm) catalyzed gas diffusion electrode in three different electrolytes under CO_2 gas flowing.

Similarly as above, the electrolyte of NaOH demonstrated the highest current density of -5.14 $mAcm^{-2}$, while the electrolyte of $CaCl_2$ obtained a current density of -4.64 $mAcm^{-2}$. Likewise, the electrolyte of $NaHCO_3$ showed a current density of -4.14 $mAcm^{-2}$. From figure 3.6 to 3.11 we arrived at some conclusions. First, the NaOH as the electrolyte revealed the highest current density at -1.7 V. Second, the current density of CO_2 bubbling at -1.7 V was lower than that of N_2 bubbling at identical conditions and setups.

B. <u>The influence of Cu_2O particles in three different morphologies on the electrochemical reaction of CO_2</u>

The Cu_2O particles with a diameter of 170 nm revealed the highest current density at -1.7 V in $NaHCO_3$ aqueous solution (shown in figure 3.12). Figure 3.13 exhibits that the Cu_2O particles with a diameter of 170 and 640 nm demonstrating similar densities of -5.5 $mAcm^{-2}$ at -1.7 V in NaOH aqueous electrolyte. When the electrochemical reactions were conducted in the $CaCl_2$ electrolyte, the Cu_2O particles with a diameter of 1570 nm showed the highest current density. This is to our surprise that the larger particles of Cu_2O resulted in higher current densities in this case (figure 3.13). Table 3.1 lists the current density at -1.7 V with different sizes of Cu_2O particles in three different electrolytes under constant N_2 or CO_2 bubbling.

C. The catalytic ability of the Cu_2O particles on the electrochemical reaction of CO_2

We observed that the electrolysis under constant N_2 bubbling arrived at higher current densities than under CO_2 bubbling. We realized that when the electrolysis was conducted under the N_2 atmosphere, at the working electrode exclusively H_2 was evolved and no CO_2 was being reduced. Hence, the current density recorded under N_2 gas bubbling was attributed solely to water reduction. The CV curves of figure 3.15 demonstrate two interesting points. First, the Cu_2O is not the catalyst for water electrolysis because there was negligible current response observed. Second, the Cu_2O itself is not reduced in the potential range from -0.4 to -1.7 V since there was no reduction peak recorded. Figure 3.16 presents the electrochemical reduction of CO_2 with and without Cu_2O in 0.5 M NaOH aqueous solution. From the CV curves we observed that the Cu_2O catalyzed the electrochemical reduction of CO_2 because a much larger current was resulted over that of non-Cu_2O electrode.

3.3.2. Result from potentiostatic measurement

A. The influence of three different electrolytes on the stability of the electrochemical reaction of CO_2

Through figure 3.17, 3.18, and 3.19 we determined that the electrochemical reactions occurring in the $CaCl_2$ electrolyte were

unstable. When the electrolyte was $NaHCO_3$ instead, the current density revealed negligible change after electrochemical reactions for 5 hours. The current density for the electrochemical reactions in the NaOH at -1.7 V became unstable for the first hour and then the current density was stabilized. From EDX we determined that the electrode in the $CaCl_2$ electrolyte was covered with calcium after 5 hours, which effectively decreased the current response (shown in figure 3.20). Table 3.2 lists the average current densities for three different Cu_2O particles in three different electrolytes under the CO_2 gas flowing at -1.7 V for 5 hours. When the NaOH was used as the electrolyte, most of the current densities recorded were higher than those of $NaHCO_3$ and $CaCl_2$. The only exception was the Cu_2O particles with a diameter of 170 nm in $NaHCO_3$, which demonstrated marginally higher current density than that in NaOH.

B. <u>The influence of Cu_2O particles in three different morphologies on the stability of the electrochemical reaction of CO_2</u>

When the $NaHCO_3$ was used as the electrolyte, the Cu_2O particles with a diameter of 170 nm resulted in the highest current density. The larger Cu_2O particles obtained the higher current densities when the $NaHCO_3$ was used as the electrolyte (shown in figure 3.21). The current densities for the Cu_2O particles with different sizes showed negligible change when the NaOH was used as the electrolyte (shown in figure 3.22). The current density for the Cu_2O particles with a diameter of 170 nm in the $CaCl_2$ electrolyte demonstrated the highest current

density about -7.3 $mAcm^{-2}$ at -1.7 V and its current decreased rapidly with the precipitation of calcium on the electrode. In the $CaCl_2$ electrolyte, the Cu_2O with particle sizes of 640 nm demonstrated more stable current density than the particle sizes of 1570 and 640 nm (shown in figure 3.23).

3.4. Conclusions

The electrochemical reductions of CO_2 with the Cu_2O catalyzed gas diffusion electrode in different electrolytes of 0.5 M at ambient temperature were studied. Combinations with Cu_2O particles in three different sizes (1570, 640, and 170 nm) and three distinct electrolytes ($NaHCO_3$, NaOH, and $CaCl_2$) were explored. The highest current density recorded was -4.82 $mAcm^{-2}$, with the condition of the Cu_2O particles at a diameter of 640 nm in the 0.5 M NaOH aqueous electrolyte for 5 hours electrochemical reduction of CO_2 at -1.7 V. The electrolyte of $NaHCO_3$ demonstrated the most stability in which the current density revealed negligible change during the electrochemical testing. The smaller Cu_2O particles resulted in higher average current density when the $NaHCO_3$ or $CaCl_2$ was used as the electrolyte. The Cu_2O particles presented notable catalytic abilities for electrochemical reduction of CO_2.

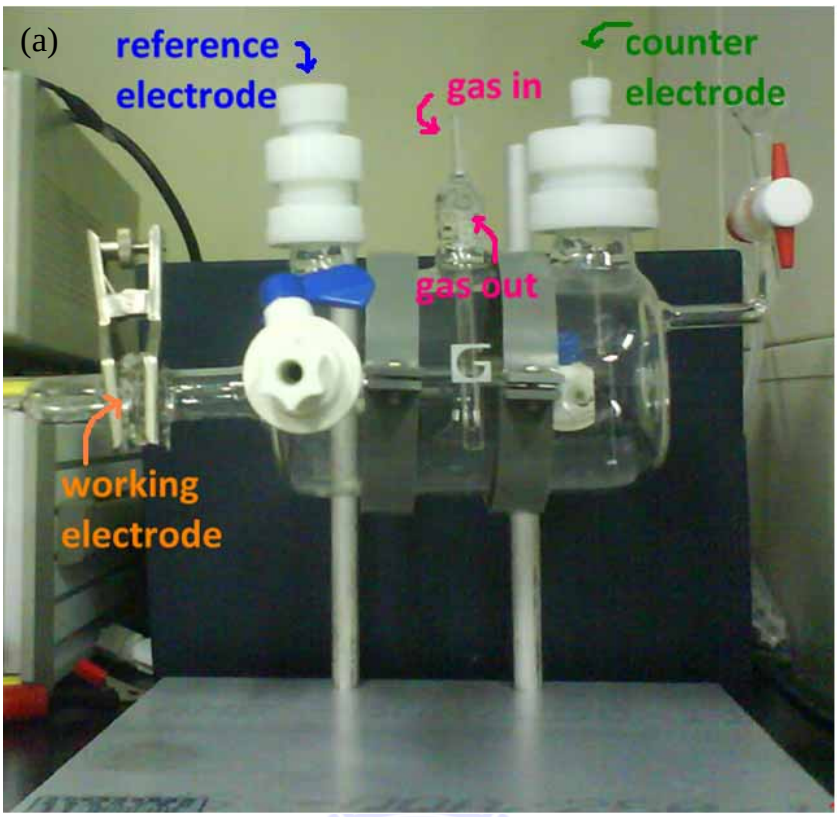

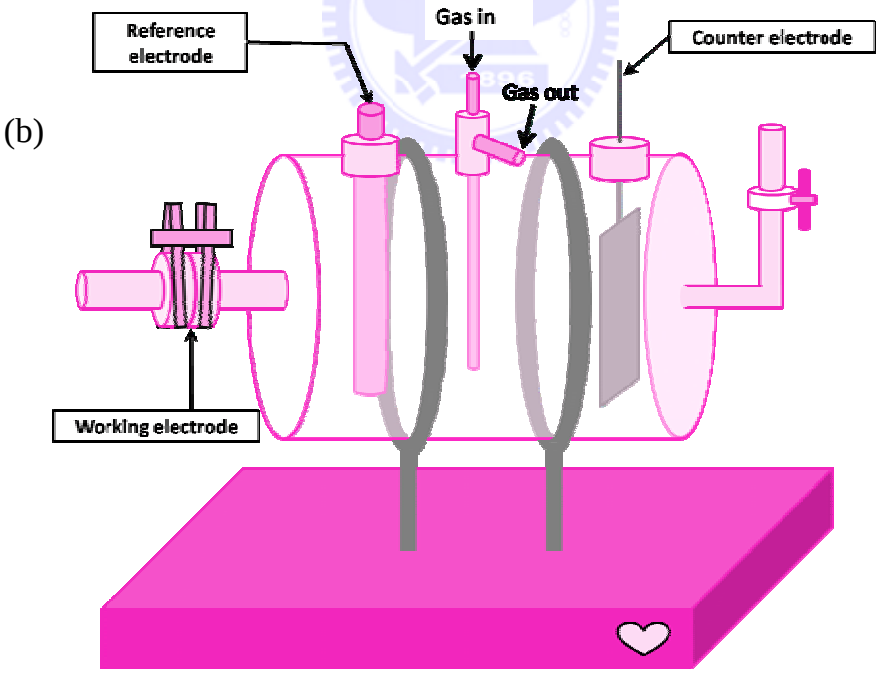

Figure 3.1. The photograph (a) and the schematic diagram (b) of the electrolysis cell.

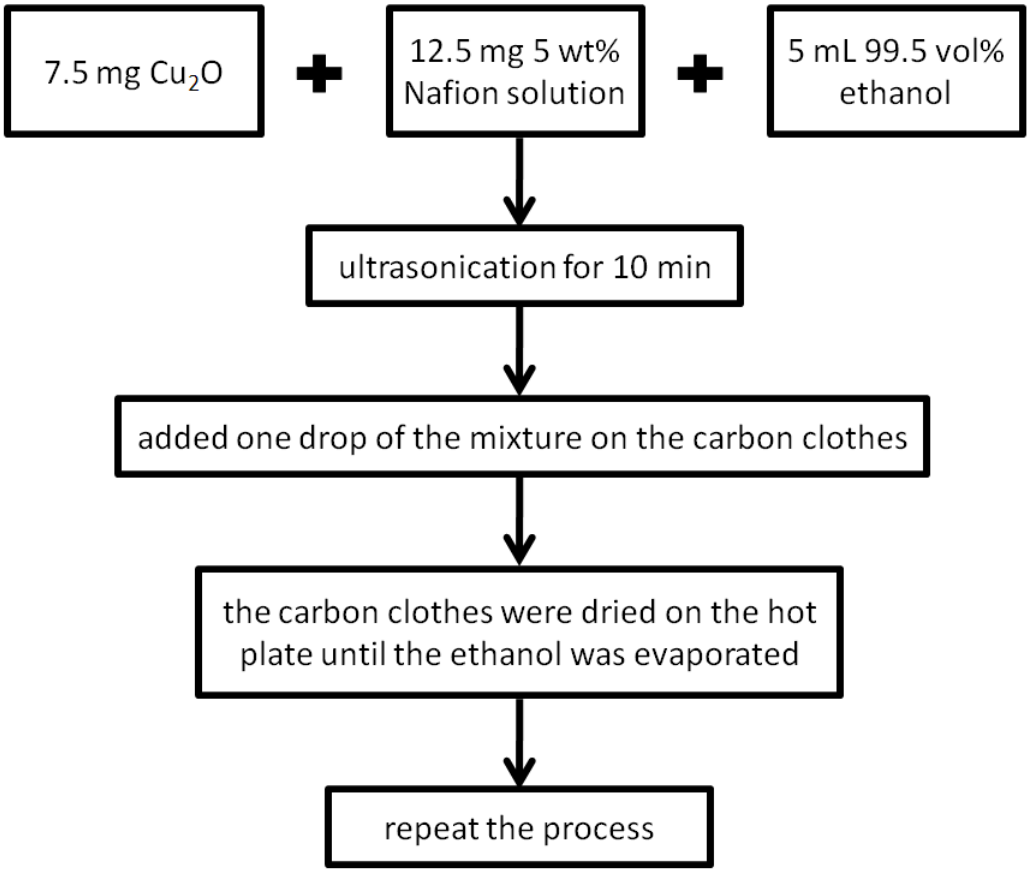

Figure 3.2. Illustration of step involved in gas diffusion electrode fabrication.

Figure 3.3. The images for the gas diffusion electrode catalyzed with the Cu_2O particles of (a) 1570, (b) 640, and (c) 170 nm.

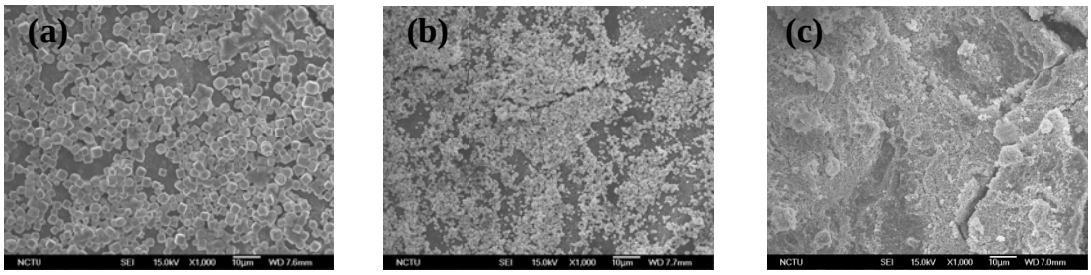

Figure 3.4. The SEM images of the gas diffusion electrode catalyzed with the Cu_2O particles of (a) 1570, (b) 640, and (c) 170 nm.

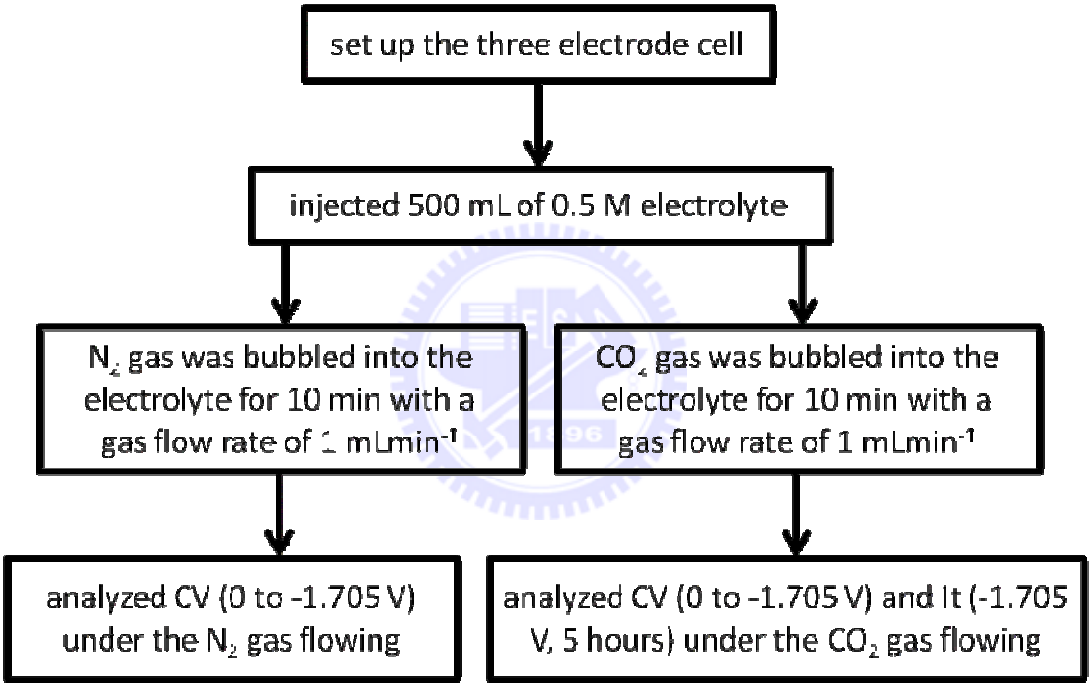

Figure 3.5. Flow chart for electrochemical analysis.

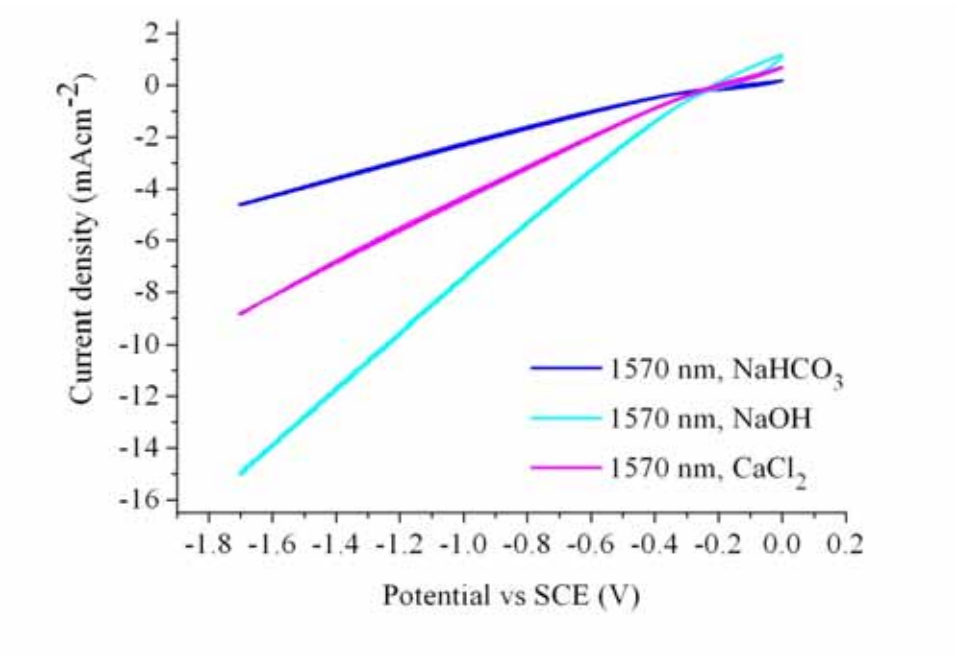

Figure 3.6. The CV curves of the electrochemical reactions catalyzed by the Cu_2O particles with a diameter of 1570 nm in different electrolytes under constant N_2 gas flowing.

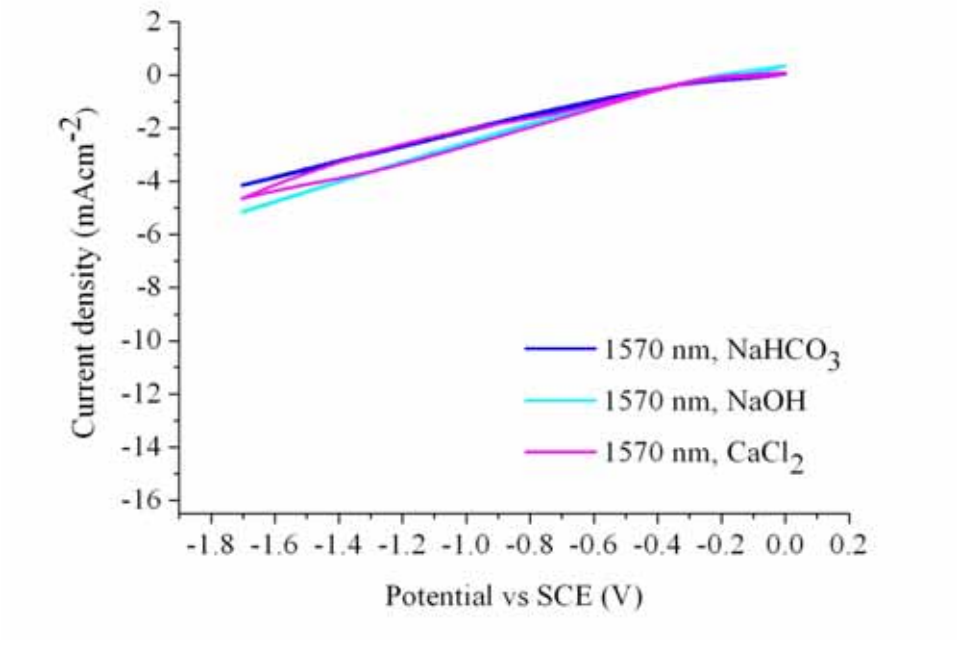

Figure 3.7. The CV curves of the electrochemical reactions catalyzed by the Cu_2O particles with a diameter of 1570 nm in different electrolytes under constant CO_2 gas flowing.

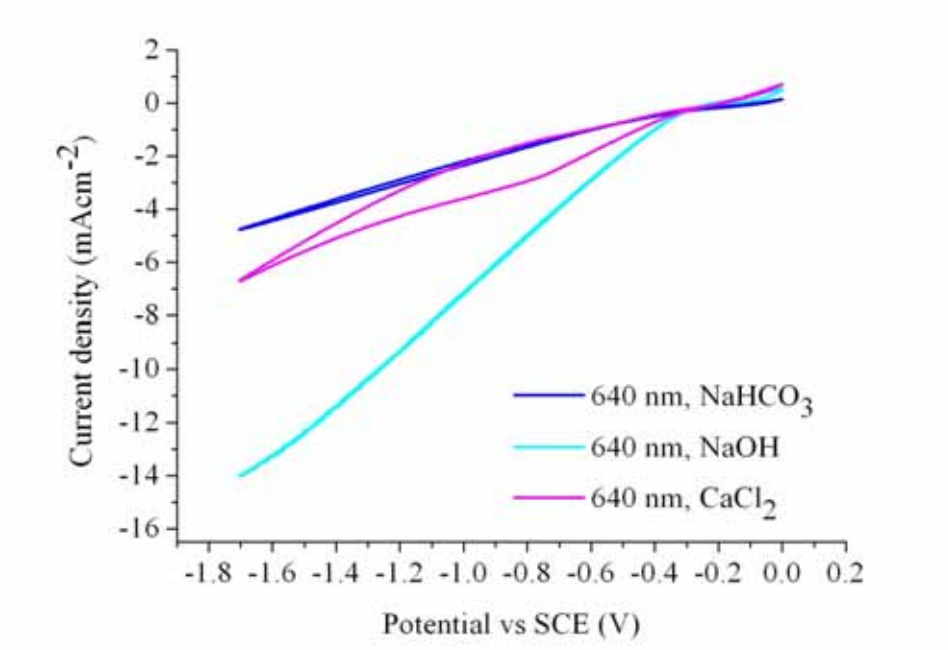

Figure 3.8. The CV curves of the electrochemical reactions catalyzed by the Cu_2O particles with a diameter of 640 nm in different electrolytes under constant N_2 gas flowing.

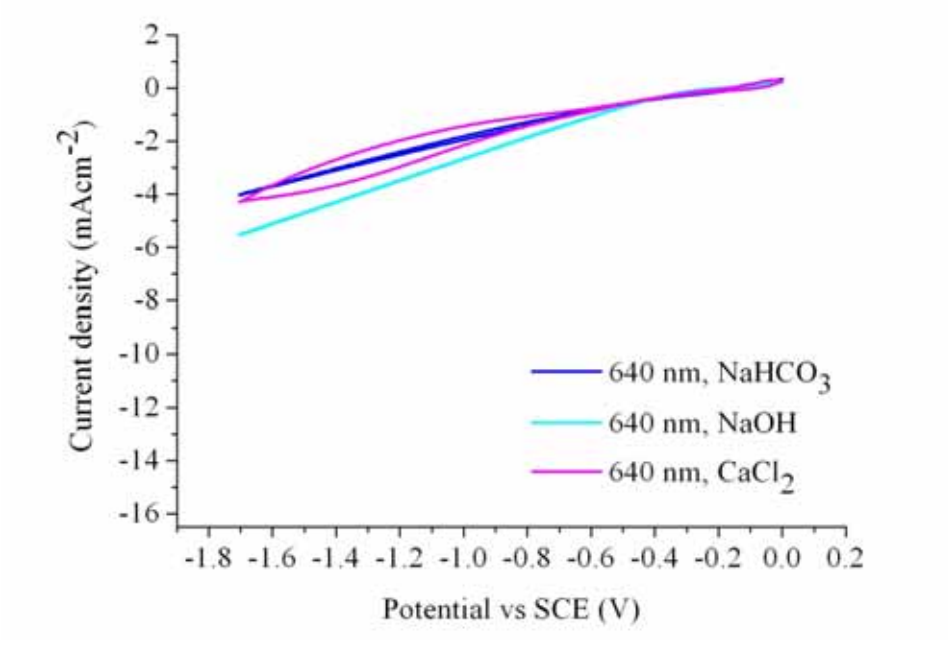

Figure 3.9. The CV curves of the electrochemical reactions catalyzed by the Cu_2O particles with a diameter of 640 nm in different electrolytes under constant CO_2 gas flowing.

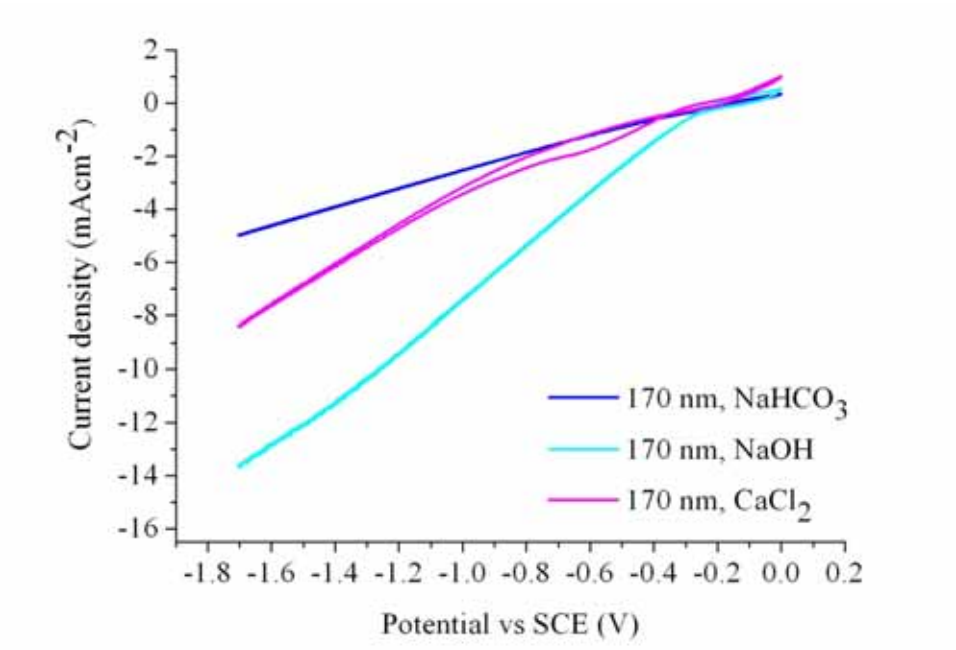

Figure 3.10. The CV curves of the electrochemical reactions catalyzed by the Cu_2O particles with a diameter of 170 nm in different electrolytes under constant N_2 gas flowing.

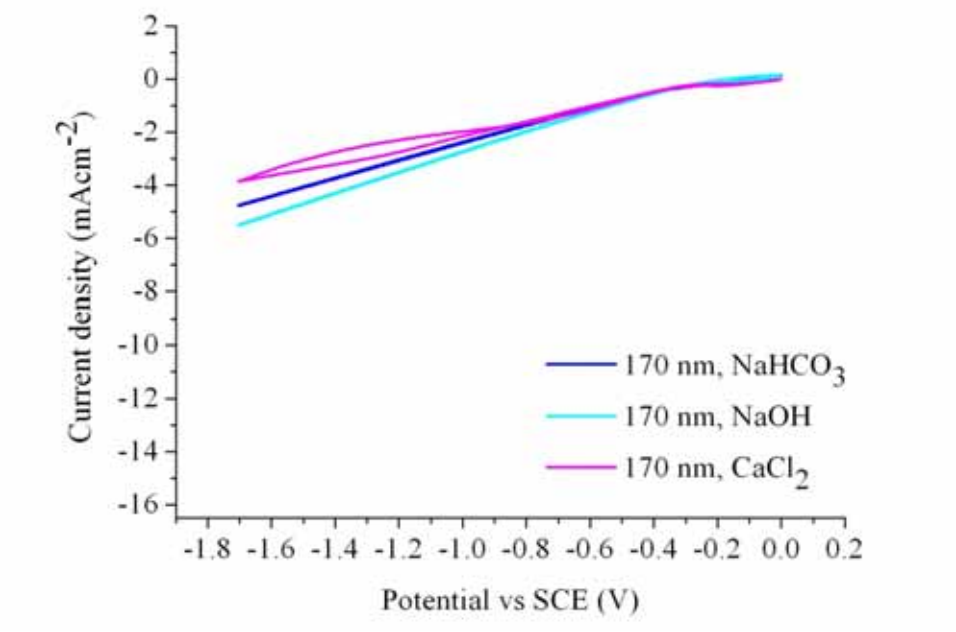

Figure 3.11. The CV curves of the electrochemical reactions catalyzed by the Cu_2O particles with a diameter of 170 nm in different electrolytes under constant CO_2 gas flowing.

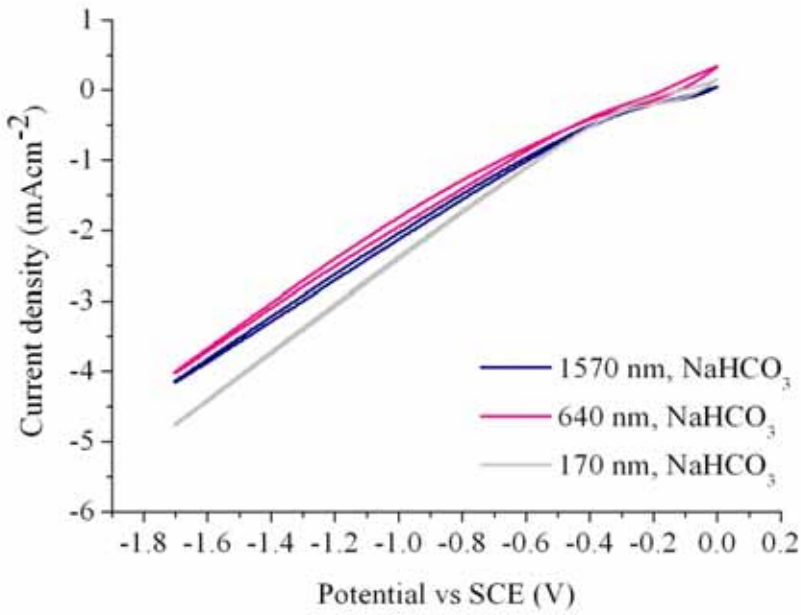

Figure 3.12. The CV curves of the electrochemical reactions catalyzed by the Cu_2O particles with different diameters in $NaHCO_3$ acted as the electrolyte under constant CO_2 gas flowing.

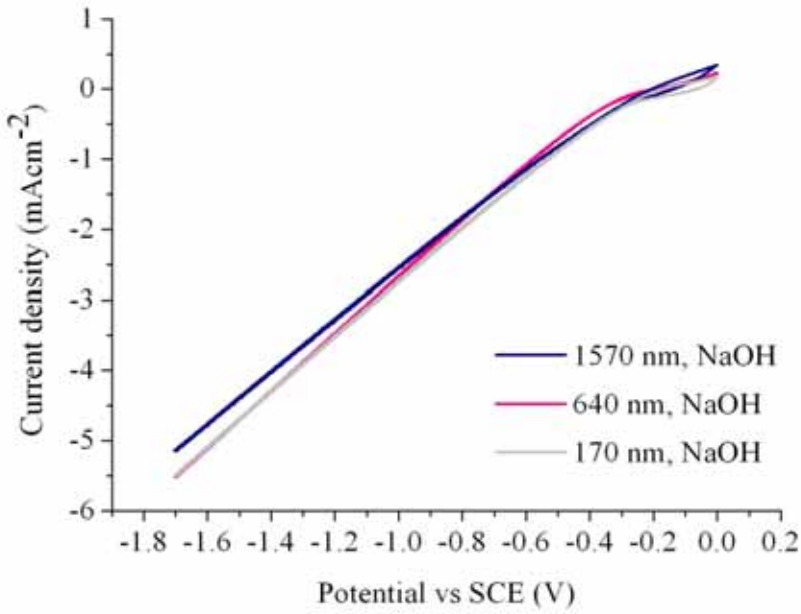

Figure 3.13. The CV curves of the electrochemical reactions catalyzed by the Cu_2O particles with different diameters in NaOH acted as the electrolyte under constant CO_2 gas flowing.

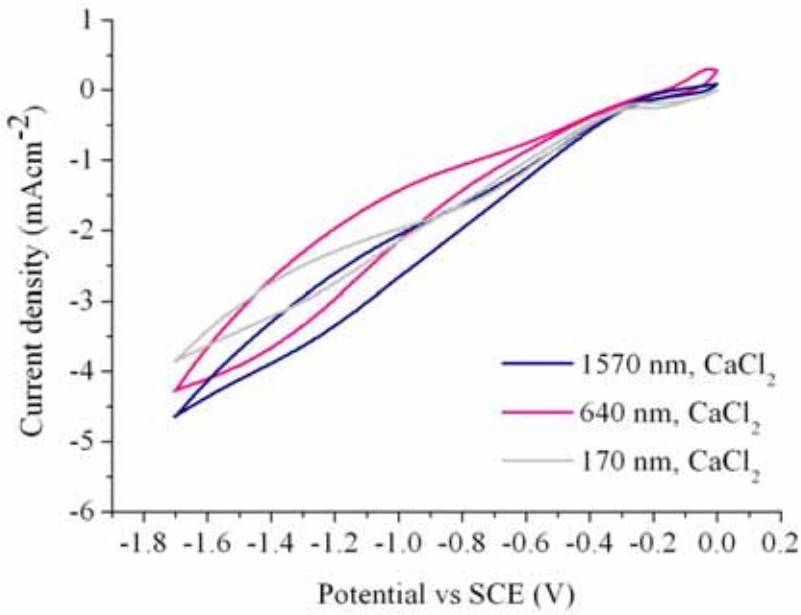

Figure 3.14. The CV curves of the electrochemical reactions catalyzed by the Cu_2O particles with different diameters in $CaCl_2$ acted as the electrolyte under constant CO_2 gas flowing.

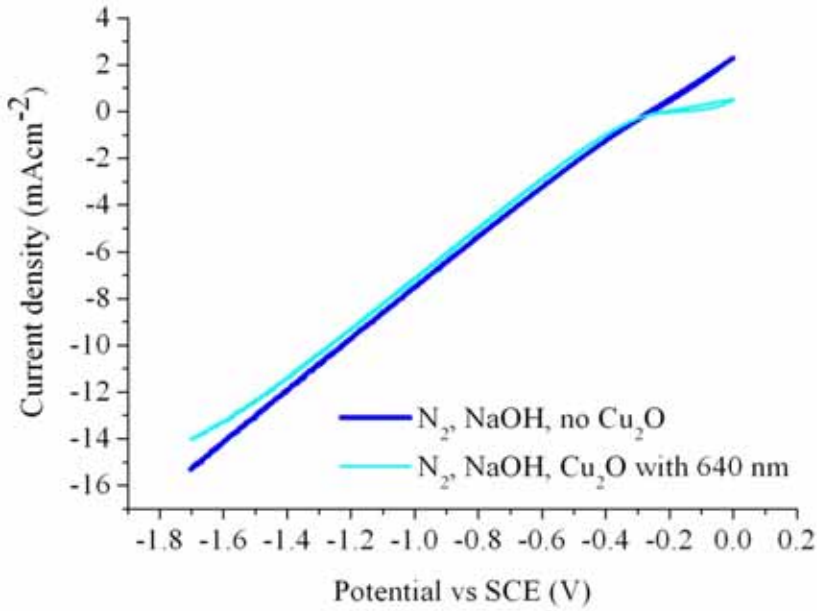

Figure 3.15. The CV curves of the electrochemical reactions with and without the Cu_2O particles in NaOH acted as the electrolyte under constant N_2 gas flowing.

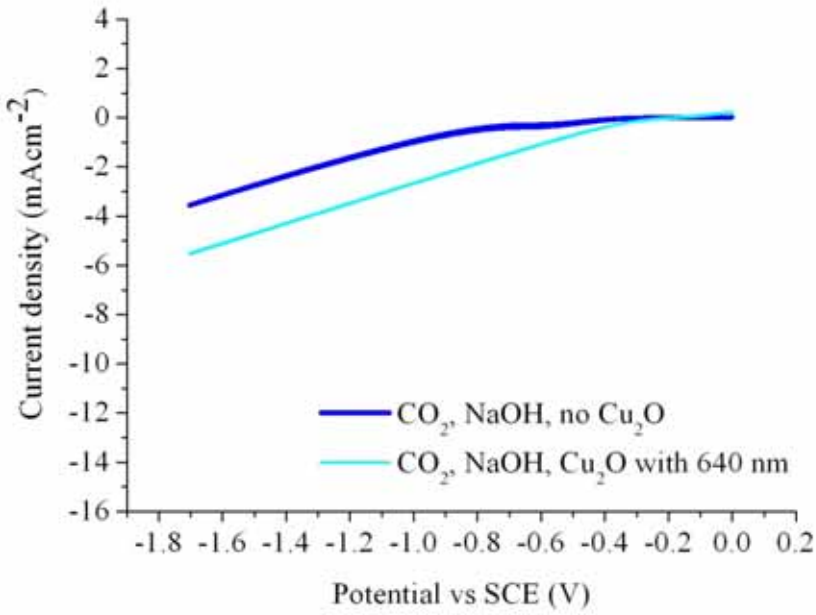

Figure 3.16. The CV curves of the electrochemical reactions with and without the Cu_2O particles in NaOH acted as the electrolyte under constant CO_2 gas flowing.

Table 3.1. The current density at -1.7 V with Cu_2O particles in different sizes in three different electrolytes under N_2 or CO_2 constant bubbling.

gas	Particle size	$NaHCO_3$	NaOH	$CaCl_2$
N_2	1570 nm	-4.61 $mAcm^{-2}$	-15 $mAcm^{-2}$	-8.82 $mAcm^{-2}$
	640 nm	-4.75 $mAcm^{-2}$	-14 $mAcm^{-2}$	-6.68 $mAcm^{-2}$
	170 nm	-4.97 $mAcm^{-2}$	-13.6 $mAcm^{-2}$	-8.36 $mAcm^{-2}$
CO_2	1570 nm	-4.14 $mAcm^{-2}$	-5.14 $mAcm^{-2}$	-4.64 $mAcm^{-2}$
	640 nm	-4.01 $mAcm^{-2}$	-5.51 $mAcm^{-2}$	-4.28 $mAcm^{-2}$
	170 nm	-4.75 $mAcm^{-2}$	-5.5 $mAcm^{-2}$	-3.85 $mAcm^{-2}$

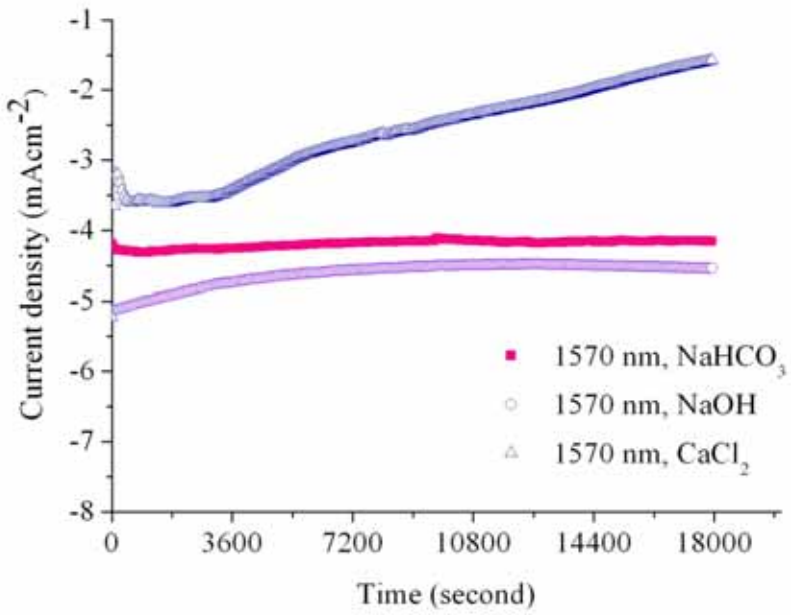

Figure 3.17. The current-time curves for the electrochemical reactions catalyzed by the Cu_2O particles with a diameter of 1570 nm in the different electrolytes under constant CO_2 gas flowing at -1.7 V.

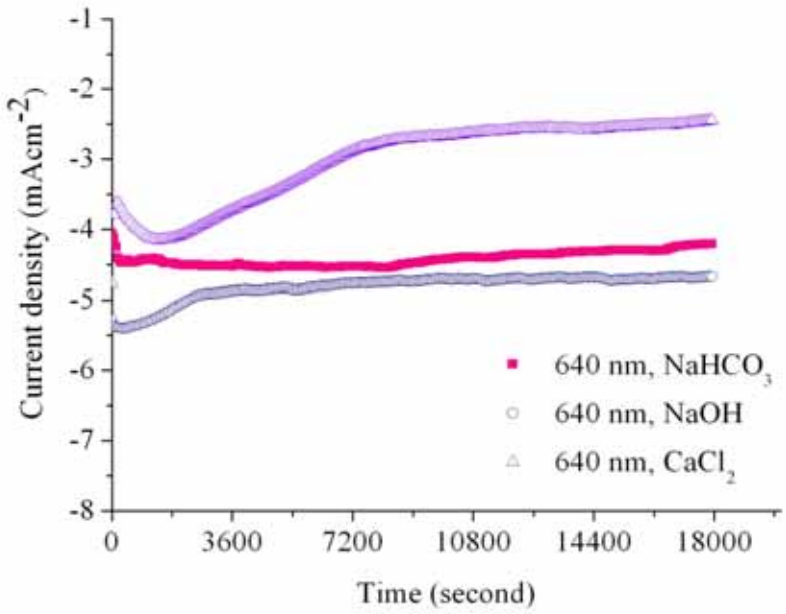

Figure 3.18. The current-time curves for the electrochemical reactions catalyzed by the Cu_2O particles with a diameter of 640 nm in the different electrolytes under constant CO_2 gas flowing at -1.7 V.

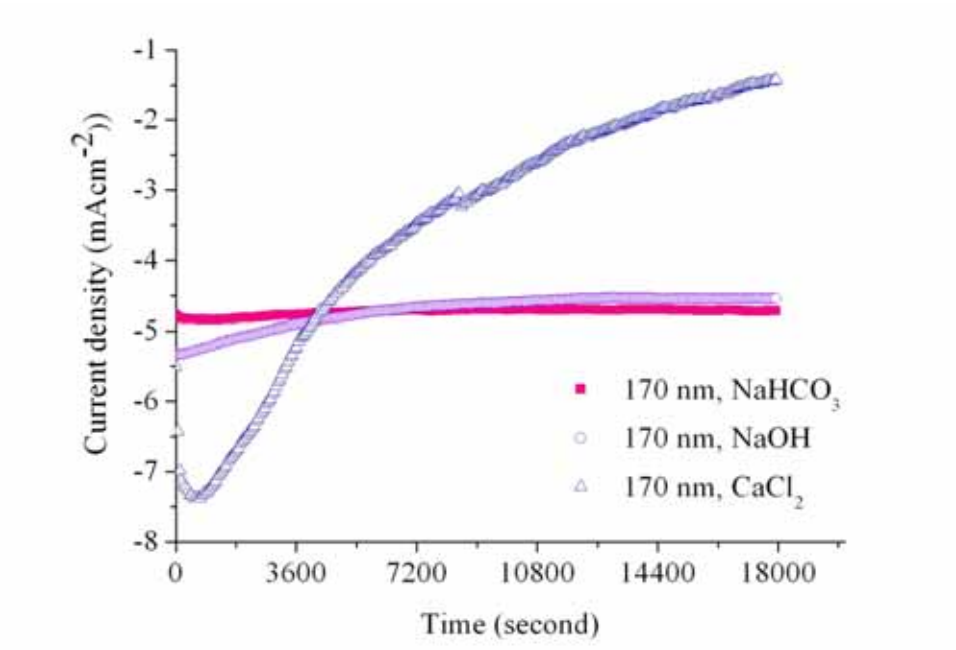

Figure 3.19. The current-time curves for the electrochemical reactions catalyzed by the Cu_2O particles with a diameter of 170 nm in the different electrolytes under constant CO_2 gas flowing at -1.7 V.

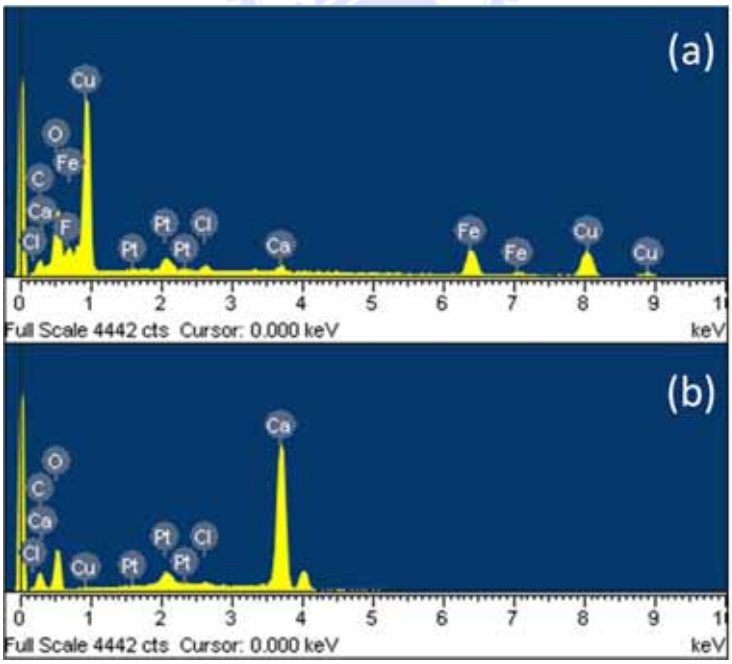

Figure 3.20. The EDX images before (a) and after (b) electrochemical reaction for 5 hours in the $CaCl_2$ electrolyte.

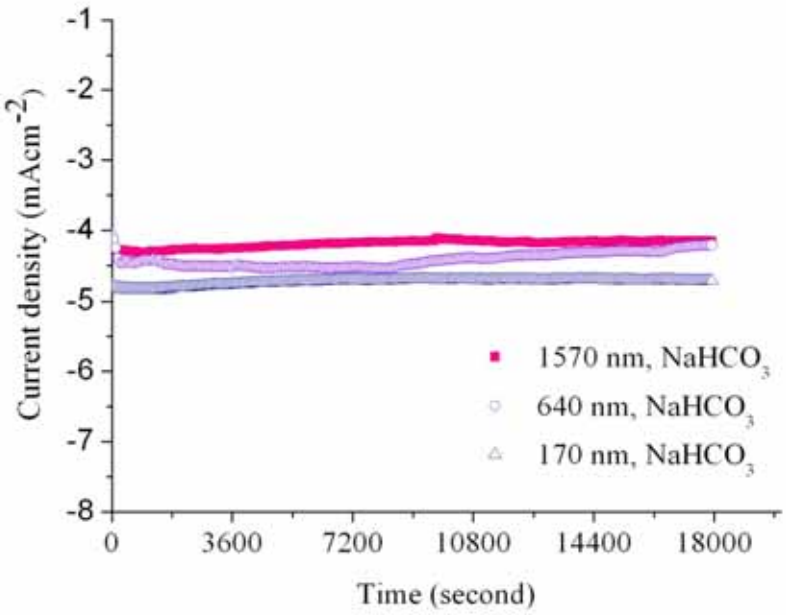

Figure 3.21. The time-current curves for the electrochemical reactions catalyzed by the Cu_2O particles with different diameters in the $NaHCO_3$ electrolyte under constant CO_2 gas flowing at -1.7 V.

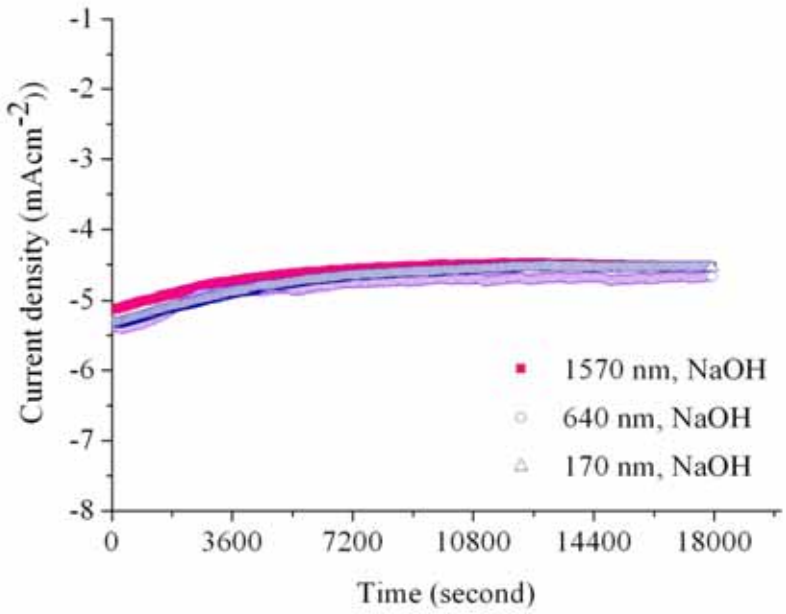

Figure 3.22. The current-time curves for the electrochemical reactions catalyzed by the Cu_2O particles with different diameters in the NaOH electrolyte under constant CO_2 gas flowing at -1.7 V.

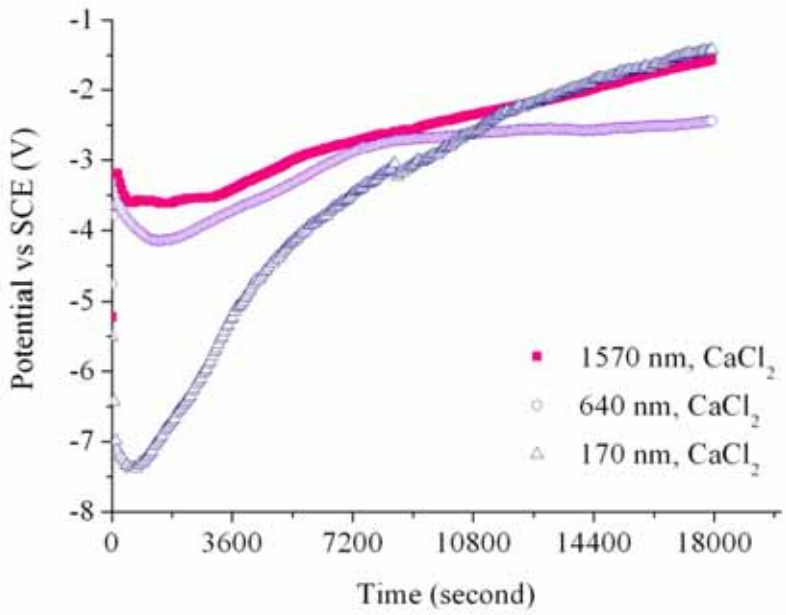

Figure 3.23. The current-time curves for the electrochemical reactions catalyzed by the Cu_2O particles with different diameters in the $CaCl_2$ electrolyte under constant CO_2 gas flowing at -1.7 V.

Table 3.2. The average current densities for the Cu_2O particles in three different sizes in three different electrolytes under the constant CO_2 gas flowing at -1.7 V for 5 hours electrochemical reaction.

	$NaHCO_3$	NaOH	$CaCl_2$
1570 nm	-4.19155 $mAcm^{-2}$	-4.61581 $mAcm^{-2}$	-2.61968 $mAcm^{-2}$
640 nm	-4.41833 $mAcm^{-2}$	-4.81755 $mAcm^{-2}$	-3.02033 $mAcm^{-2}$
170 nm	-4.73211 $mAcm^{-2}$	-4.72106 $mAcm^{-2}$	-3.533 $mAcm^{-2}$

Chapter 4.

Photocatalytic Properties of Cuprous Oxide

4.1. Introduction

Photocatalysis is the phenomenon that occurs on the surface of a semiconductor by the photoinduced electron-hole pairs. Photocatalyst is a material that is used to accelerate the desired photoreaction. In chapter 1 we have already described some semiconductors that could act as photocatalysts. The most widely known photocatalyst is TiO_2, which promotes the photochemical reaction of some organic and inorganic compounds only under UV light region. The Cu_2O as a semiconductor with a direct bandgap of 2.14 eV is expected to accelerate the photoreaction of some organic or inorganic compounds under visible light irradiation.

We have already discussed methods in fabricating different sizes and shapes of Cu_2O particles in chapter 2. In this chapter, we concentrate on the effect of the photocatalysts morphologies and light sources on the photocatalysis processes in Cu_2O. The Cu_2O particles with diameters of 1570, 640, and 170 nm were chosen as photocatalysts. Photocatalytic degradation of methyl orange in an aqueous solution containing the Cu_2O was investigated under one 150 W halogen lamp (yellow light), or two to four 27 W fluorescent lamp (white light). The photocatalytic efficiencies were estimated by recording the primary absorption peak of methyl orange with a UV-Vis spectrophotometer. We determined that the photochemical process catalyzed by Cu_2O particle with a diameter of 170 nm under single 150 W halogen lamp

demonstrated the highest photocatalytic efficiency.

The materials and the photocatlytic processes of Cu_2O particles are mentioned in the experimental section (Section 4.2). The degradation abilities of the photocatalysts with three different morphologies are discussed in section 4.3. The conclusions for this work are provided in section 4.4.

4.2. Experimental

4.2.1. Reagents

1. As-prepared Cu_2O particles with a diameter of 1570 nm

   Method: method A and aging for 6 hours

   Reagents: $CuCl_2$ (0.005 M), PEG (200) (2 M), NaOH (2 M), and LAAS (0.05 M)

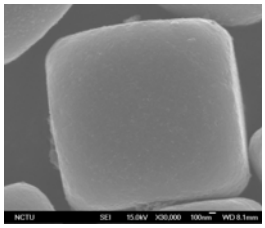

2. As-prepared Cu_2O particles with a diameter of 640 nm

   Method: method A and aging for 6 hours

   Reagents: $CuCl_2$ (0.005 M), PEG (200) (0.002 M), NaOH (0.2 M), and LAAS (0.05 M)

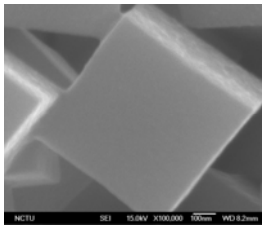

3. As-prepared Cu_2O particles with a diameter of 170 nm

   Method: method A and aging for 6 hours

   Reagents: $CuCl_2$ (0.005 M), PEG (200) (0.002 M), NaOH (0.02 M), and LAAS (0.05 M)

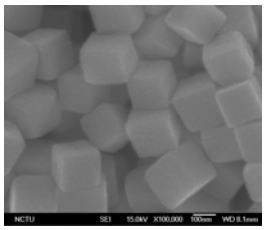

4. Methyl Orange FluKa

4.2.2. Determination in photocatalytic ability

10 mg of the Cu_2O particles was put into the vessel covered with an aluminum foil. 100 mL of 10 mgL^{-1} methyl orange (MeO) solution was added to the vessel followed by ultrasonication for 30 min in darkness. The samples were irradiated with light from a 150 W halogen lamp or four to two 27 W fluorescent lamps. The distance between the sample and light source was 5 cm. Photocatalysis results were evaluated by detecting the absorbance of the solutions with a dual beam UV-Vis spectrophotometer (HITACHI U-3300 Spectrophotometer) at 464 nm, which is the maximum absorbance of MeO.

4.3. Results and discussion

In this section, we discuss the influence of the particles morphologies and light sources on the photocatalytic process.

4.3.1. The influence of the catalysts on the degradation ability of methyl orange

The Cu_2O particles in three different diameters of 1570, 640, and 170 nm were used as the photocatalysts. As shown in figure 4.2, 4.3, and 4.4 we determined that the Cu_2O particles with a diameter of 1570 nm did not possess the ability to accelerate the desirable photochemical reaction since there was negligible reduction in the absorption peak at 464 nm. Fesult from figure 4.5, 4.6, and 4.7 suggested that the Cu_2O particles with a diameter of 640 nm revealed limited catalytic ability because the MeO absorption peak was not

reduced notably after 6 hours of irradiation under different light sources. In contrast, we obtained the information that the Cu_2O particles with a diameter of 170 nm exhibited considerable photocatalytic abilities from figure 4.8, 4.9, and 4.10. The Cu_2O particles with a diameter of 170 nm revealed the highest photocatalytic ability under the irradiation of one 150 W halogen lamp. After 6 hours in irradiation, 31.7 % of MeO was decolorized. Result from figure 4.2 to 4.10 indicated that the morphologies of the Cu_2O particles played an important role in the photochemical reaction. As expected, the particles with the smallest size provided the highest photocatalytic ability.

4.3.2. The influence of light on the degradation ability of methyl orange

Three different light sources were explored to estimate the influence of the irradiation energy on the degradation ability of MeO. Figure 4.11 provides the results for the degradation of MeO catalyzed by Cu_2O particles with a diameter of 170 nm under a single 150 W halogen lamp. We determined the degradation of MeO was 68.3 %. The Cu_2O particles with a diameter of 1570 and 640 nm did not possess photocatalytic ability under one 150 W halogen lamp. As shown in figure 4.12 and 4.13 we obtained the results that there was minimum photochemical reaction when the Cu_2O particles with diameters of 1570 and 640 nm were tested under four or two 27 W fluorescent lamps irradiations. The 27.7 % MeO decolorization was obtained by using the Cu_2O particle with diameter of 170 nm under four florescent lamps irradiation. When the lamps were reduced from four to two, the decolorization of MeO was decreased from 27.7 to 5.5 %. As shown in figure 4.14, higher irradiation energy led to higher degradation ability, which is entirely expected.

4.4. Conclusions

After careful analysis, we arrived at several conclusions. First, the Cu_2O particles with a diameter of 170 nm presented higher photocatalytic abilities than those of diameters in 640 and 1570 nm. Second, the irradiation energy influenced the photochemical reaction. When the Cu_2O particles with diameters of 640 and 1570 nm were employed as photocatalysts, the colors of the MeO solutions revealed negligible change after 6 hours of irradiation under different light sources. The highest degradation of MeO was acquired when the MeO solution containing the Cu_2O particle with a diameter of 170 nm was irradiated under one 150 W halogen lamp for 6 hours.

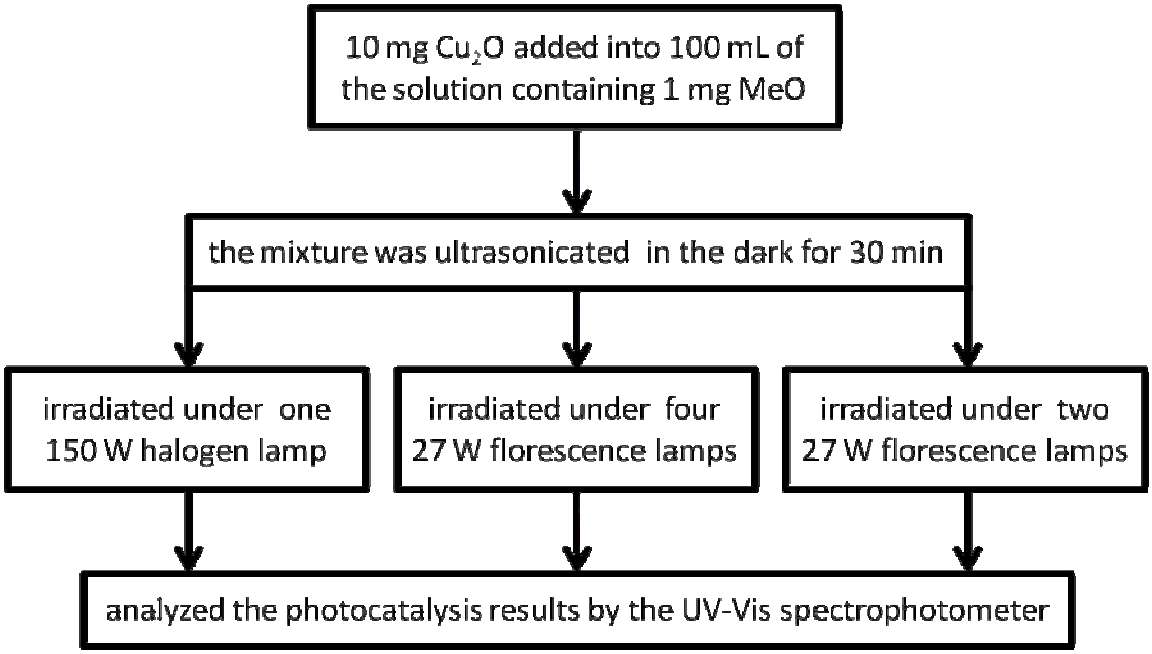

Figure 4.1. Illustration of experimental determination in photocatalytic ability.

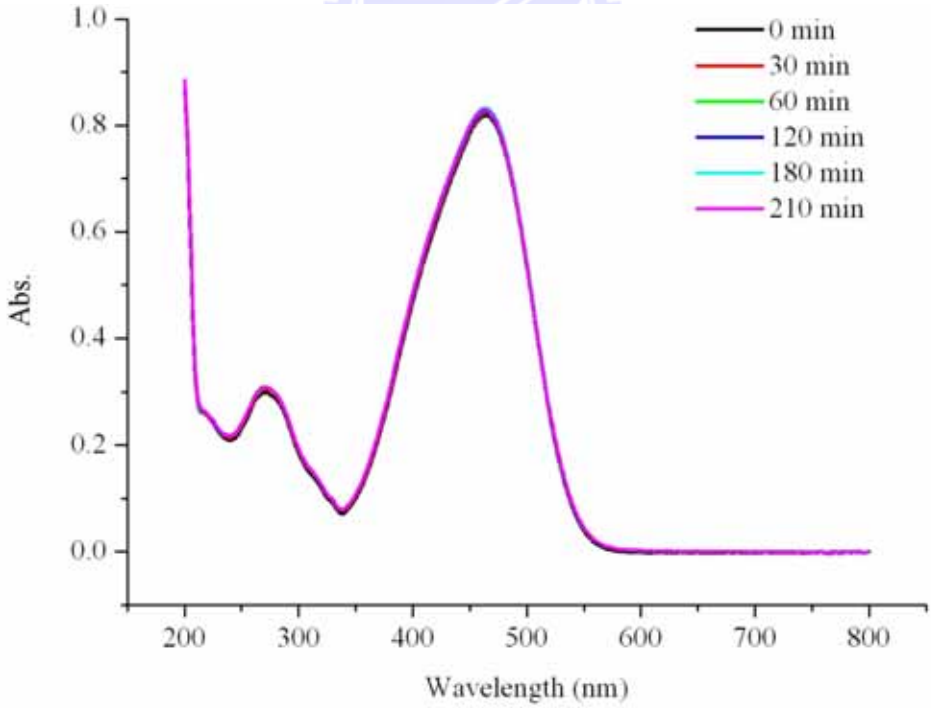

Figure 4.2. The photocatalytic ability of Cu_2O particles with a diameter of 1570 nm under one 150 W halogen lamp.

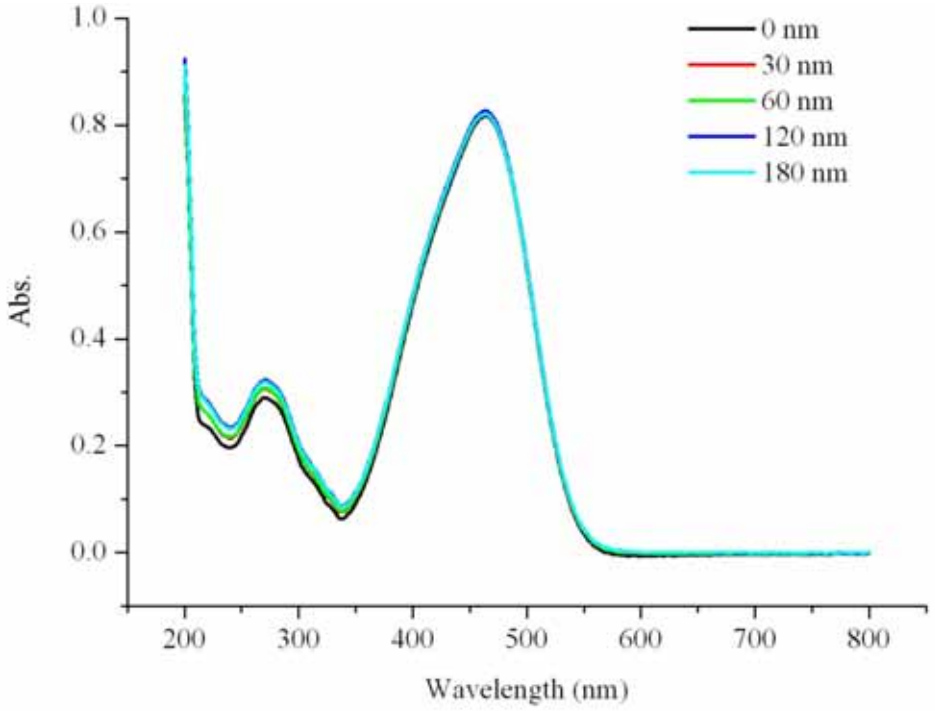

Figure 4.3. The photocatalytic ability of Cu_2O particles with a diameter of 1570 nm under four 27 W fluorescent lamps.

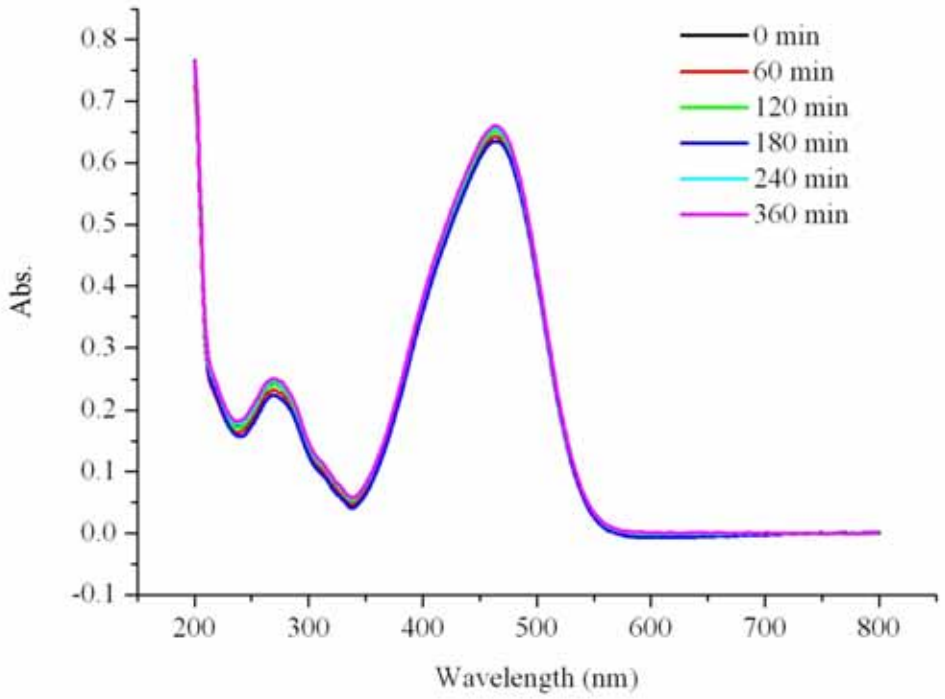

Figure 4.4. The photocatalytic ability of Cu_2O particles with a diameter of 1570 nm under two 27 W fluorescent lamps.

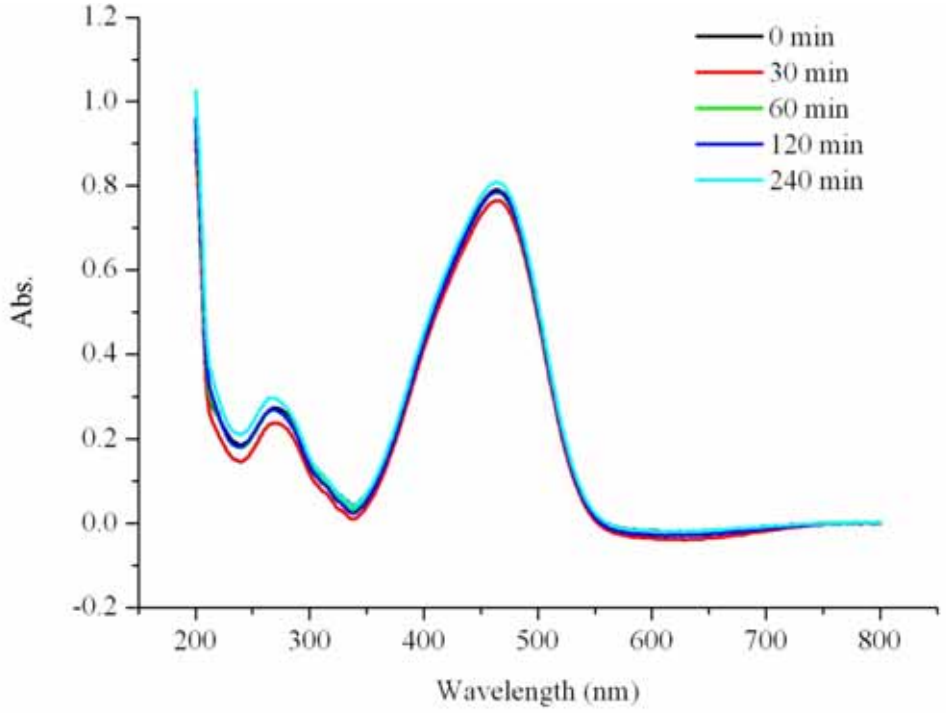

Figure 4.5. The photocatalytic ability of Cu_2O particles with a diameter of 640 nm under one 150 W halogen lamp.

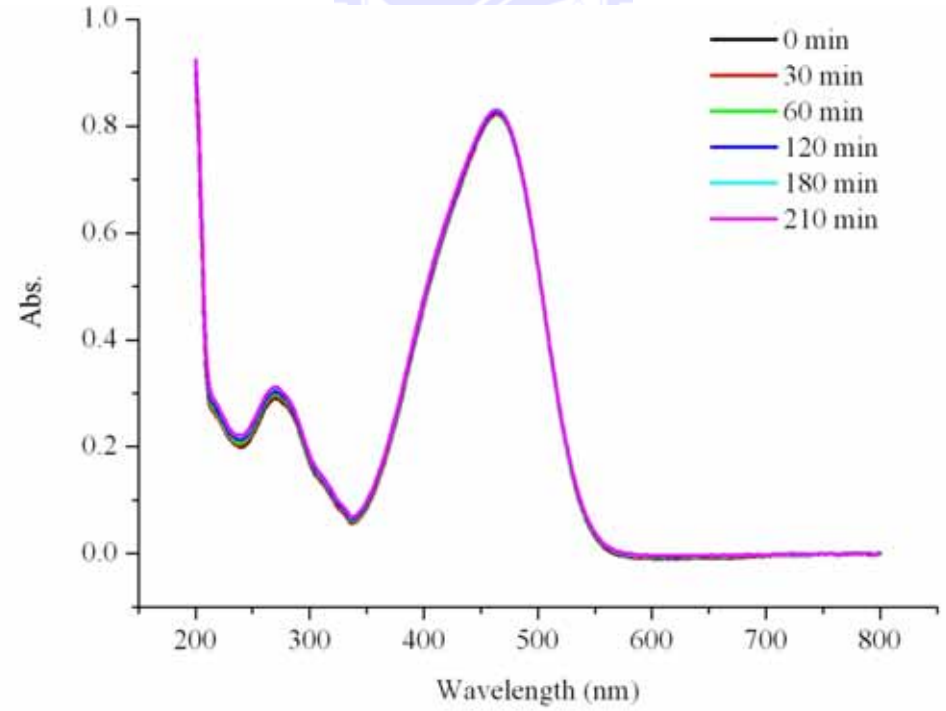

Figure 4.6. The photocatalytic ability of Cu_2O particles with a diameter of 640 nm under four 27 W fluorescent lamps.

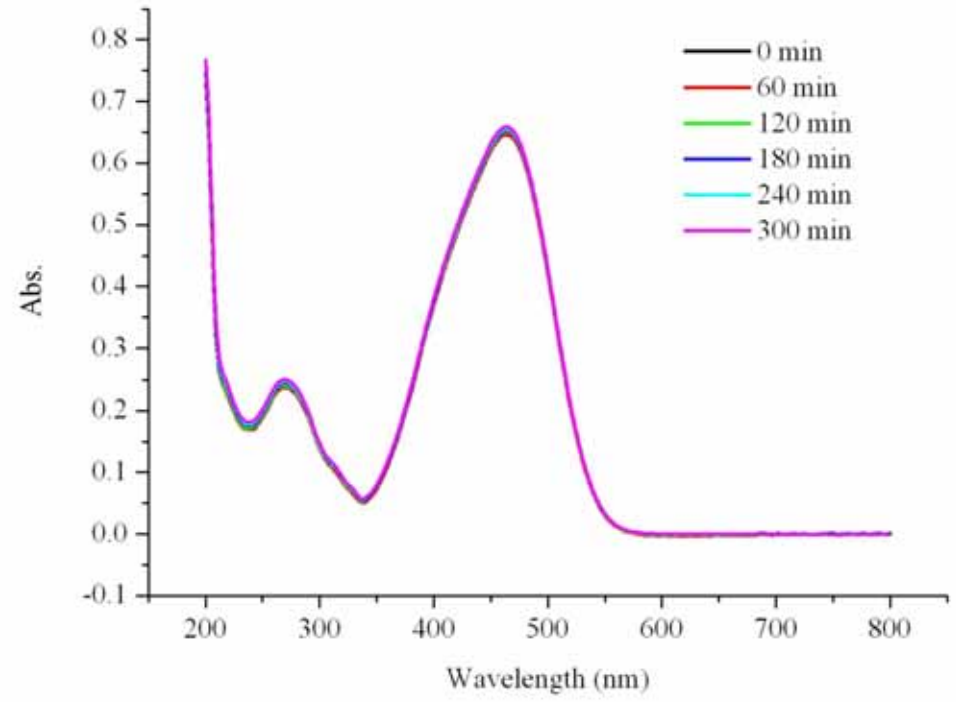

Figure 4.7. The photocatalytic ability of Cu_2O particles with a diameter of 640 nm under two 27 W fluorescent lamps.

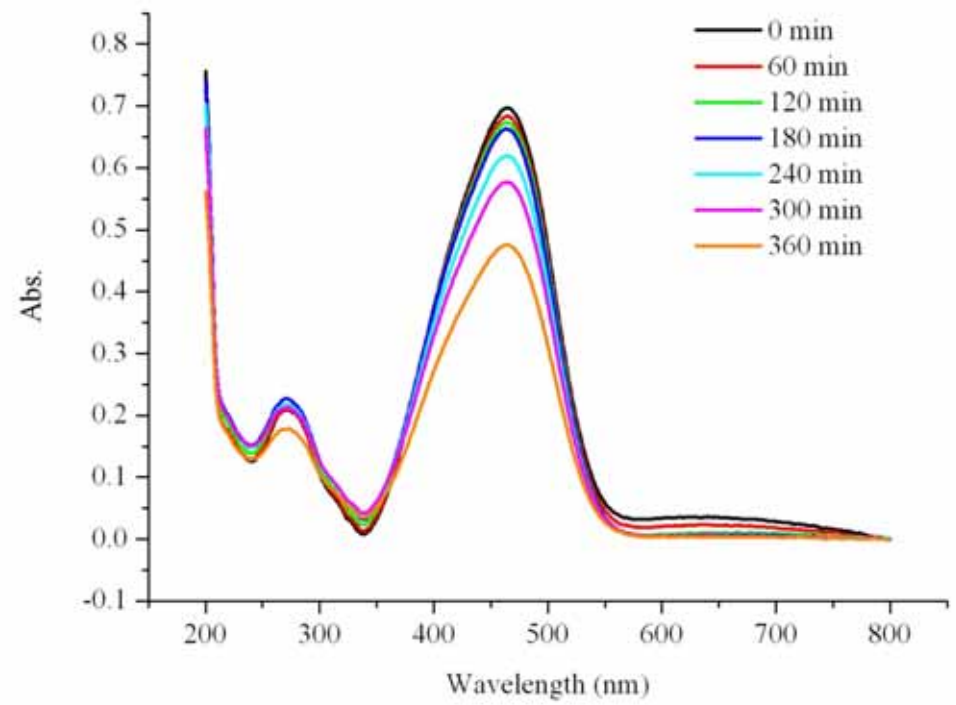

Figure 4.8. The photocatalytic ability of Cu_2O particles with a diameter of 170 nm under one 150 W halogen lamp.

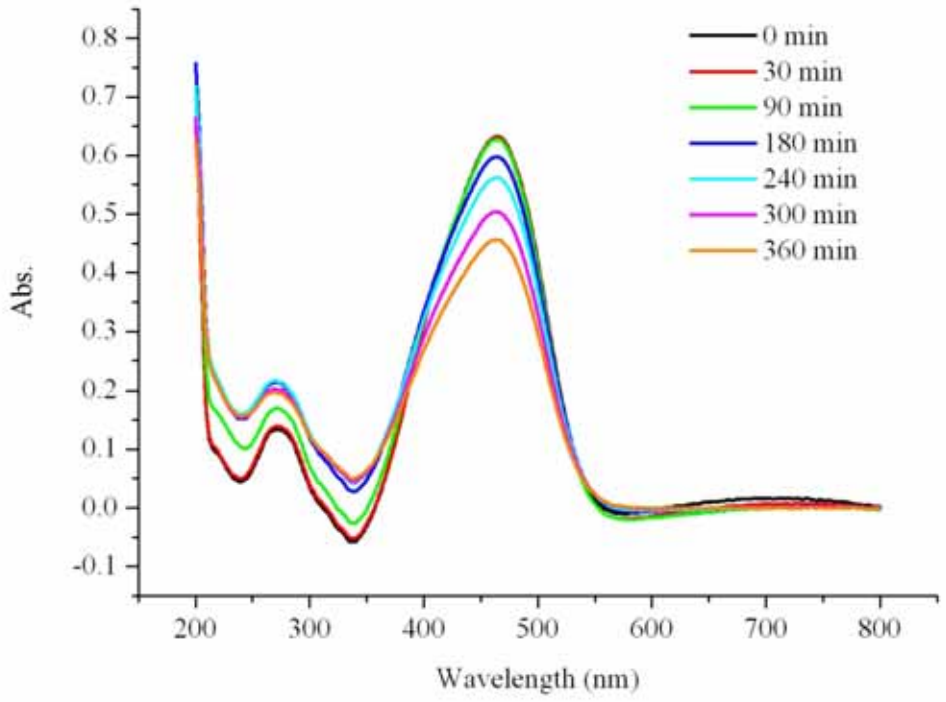

Figure 4.9. The photocatalytic ability of Cu_2O particles with a diameter of 170 nm under four 27 W fluorescent lamps.

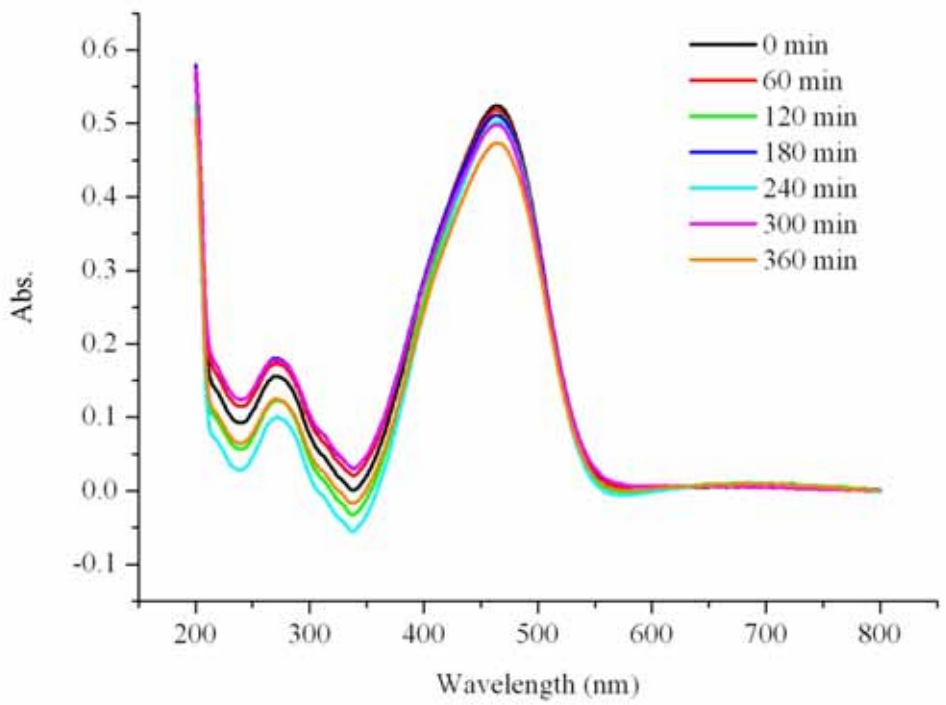

Figure 4.10. The photocatalytic ability of Cu_2O particles with a diameter of 170 nm under two 27 W fluorescent lamps.

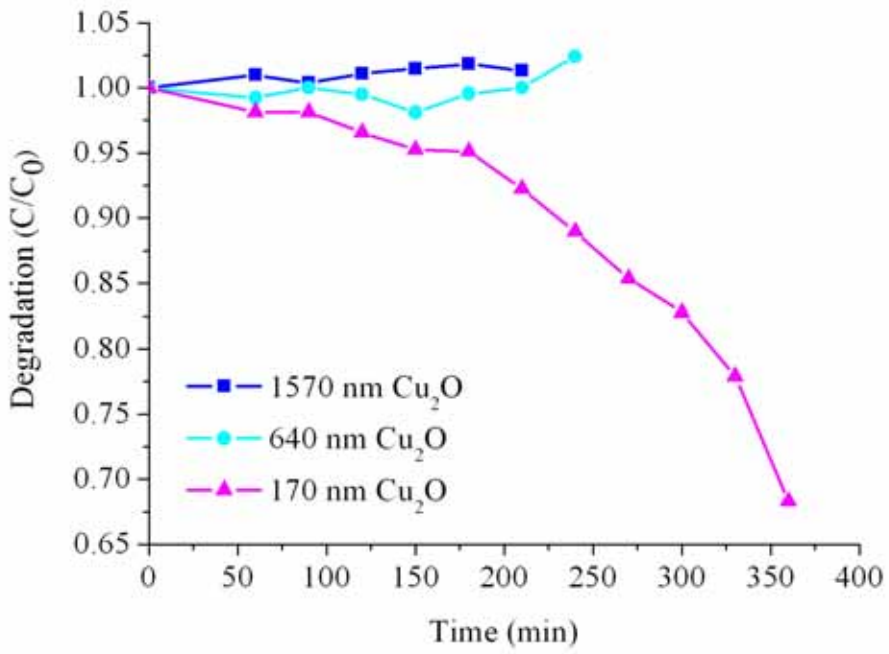

Figure 4.11. The degradation of MeO with Cu_2O particles as the photocatalysts under one 150W halogen lamp.

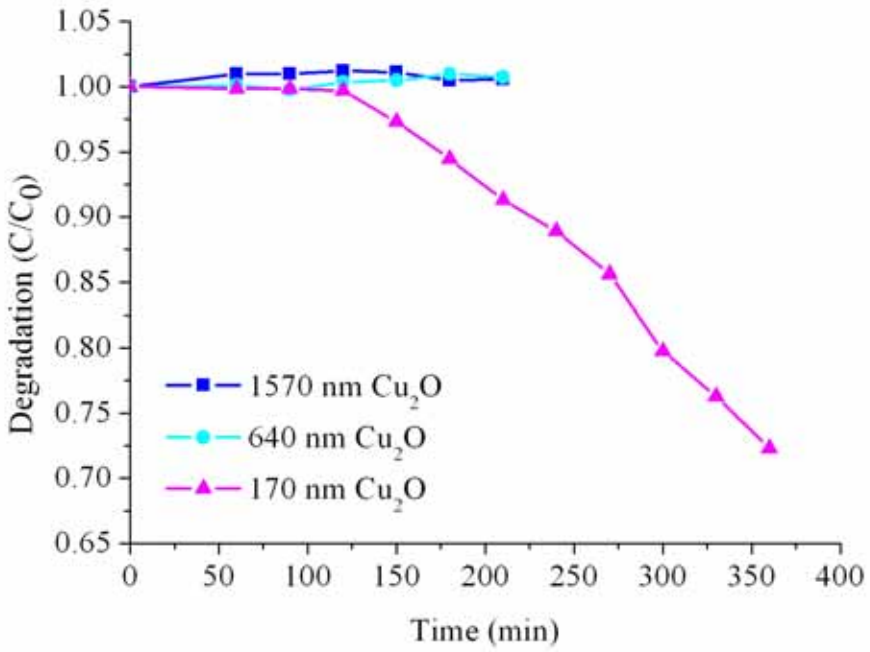

Figure 4.12. The degradation of MeO with Cu_2O particles as the photocatalysts under four 27 W fluorescent lamps.

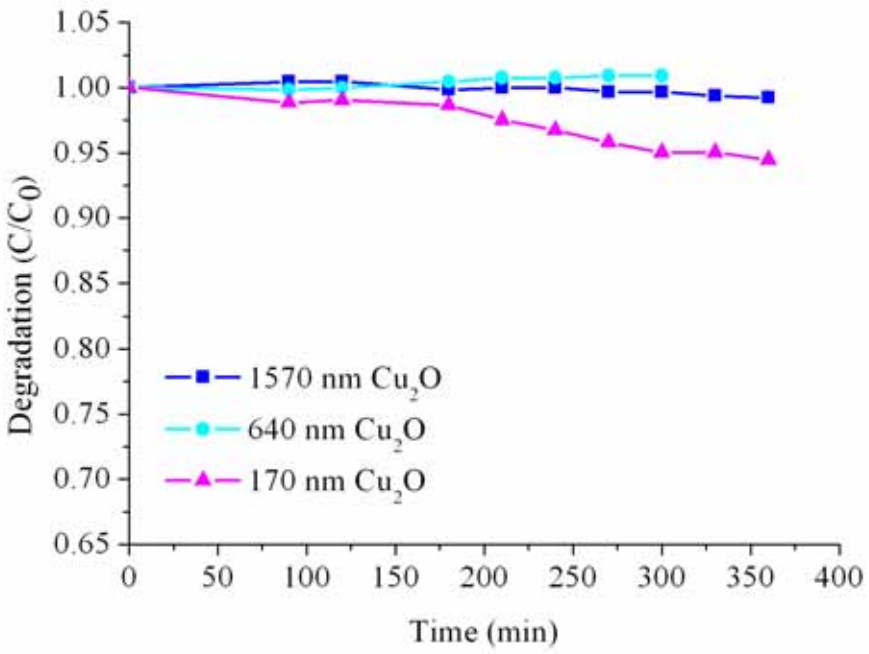

Figure 4.13. The degradation of MeO with Cu_2O particles as the photocatalysts under two 27 W fluorescent lamps.

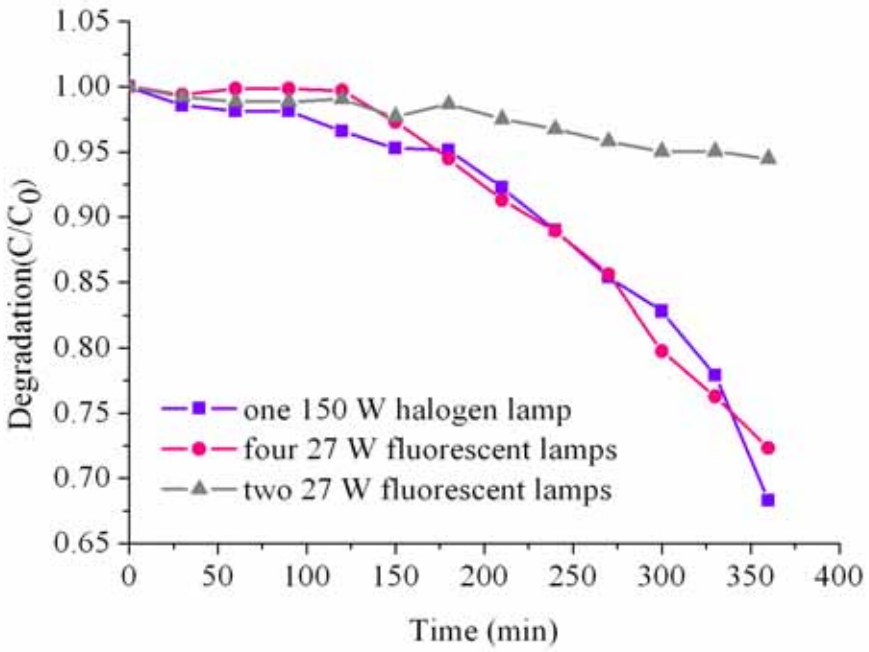

Figure 4.14. The degradation of MeO catalyzed by Cu_2O particles with diameter of 200 nm under different light sources.

Chapter 5.

Summaries and Future Work

In summary, we have successfully synthesized monodispersed Cu_2O particles with average sizes of 170, 640, and 1570 nm. In our synthetic route, changing the concentration of the PEG (200) exerted negligible influence over the particle sizes of the Cu_2O. On the contrary, adjusting the pH value of the precursor solution lead to distinct particle sizes, a fact attributed to differences in copper ion sources. In addition, the adding sequence of NaOH and LAAS solution determined the morphologies of Cu_2O particles.

The as-prepared Cu_2O particles were used to catalyze the electrochemical reduction of CO_2 and photodegradation of methyl orange. In CO_2 reduction, the highest current density recorded was -4.82 $mAcm^{-2}$, under the condition of the Cu_2O particles with a diameter of 640 nm in the 0.5 M NaOH aqueous electrolyte for 5 hours electrochemical reduction of CO_2 at -1.7 V. After carrying out identical testing with reference materials, we determined that the Cu_2O particles indicated moderate catalytic abilities for electrochemical reduction of CO_2. The highest degradation of methyl orange was acquired with the methyl orange solution containing the Cu_2O particle with a diameter of 170 nm under single 150 W halogen lamp irradiation. After 6 hours in irradiation, 31.7 % of methyl orange was decolorized.

In future work, the pH value of the solution can be optimized to obtain the Cu_2O particles as small as possible. Similarly, to find the best parameter for the electrochemical reduction of CO_2 it is better to supply the CO_2 externally to the backside of the gas diffusion electrode. In addition, complete analysis of

the reduction products from the electrochemical reaction of CO_2 is definitely necessary. Lastly, there could be other applications for the Cu_2O particles that deserve further studies.

References

1. A. E. Rakhshani, Solid-State Electronics, 1986, 1, 7.
2. A. Butts, Copper; the science and technology of the metal, its alloys and compounds, 1970, 402.
3. L. Huang, H. Wang, Z. Wang, A. Mitra, D. Zhao, and Y. Yan, Chem. Mater., 2002, 14, 876.
4. F. Sun, Y. Guo, W. Song, J. Zhao, L. Tang, and Z. Wang, Journal of Crystal Growth, 2007, 304, 425.
5. W. Wang, G. Wang, X. Wang, Y. Zhan, Y. Liu, and C. Zheng, Adv. Mater., 2002, 14, 67.
6. L. Gou and C. J. Murphy, J. Mater. Chem., 2004, 14, 735.
7. L. Xu, X. Chen, Y. Wu, C. Chen, W. Li, W. Pan, and Y. Wang, Nanotechnology, 2006, 17, 1501.
8. C. H. Kuo, C. H. Chen, and M. H. Huang, Adv. Funct. Mater., 2007, 17, 3773.
9. H. Zhang, Q. Zhu, Y. Zhang, Y. Wang, L. Zhao, and B. Yu, Adv. Funct. Mater., 2007, 17, 2766.
10. S. L. Xu, X. Y. Song, C. H. Fan, G. Z. Chen, W. Zhao, T. You, and S. X. Sun, Journal of Crystal Growth, 2007, 305, 3.
11. M. Wei, N. Lun, X. Ma, and S. Wen, Materials Letter, 2007, 61,2147.
12. J Ramirez-Ortiz, T Ogura, J Medina-Valtierra, S. E. Acosta-Ortiz, P. Bosch, J. A. de los Reyes, and V. H. Lara, Applied Surface Science, 2001, 174, 177.
13. M. Hara, T. Kondo, M. Komoda, S. Ikeda, K. Shinohara, A. Tanaka, J. N.

Kondo, and K. Domen, Chem. Commun., 1998, 357.

14. J. Zhang, J. Liu, Q. Peng, X. Wang, and Y. Li, Chem. Mater., 2006, 18, 867.
15. H. Xu, W. Wang, and W. Zhu, J. Phys. Chem. B, 2006, 110, 13829.
16. T. Minami, T. Miyata, K. Ihara, Y. Minamino, and S. Tsukada, Thin Solid Films, 2006, 494, 47.
17. L. J. Fu, J. Gao, T. Zhang, Q. Cao, L. C. Yang, Y. P. Wu, and R. Holze, Journal of Power Sources, 2007, 171, 904
18. B. White, M. Yin, A. Hall, D. Le, S. Stolbov, T. Rahman, N. Turro, and S. O'Brien, Nano Lett., 2006, 6, 2095.
19. H. A. Mosqueda, C. Vazquez, P. Bosch, and H. Pfeiffer, Chem. Mater., 2006, 18, 2307.
20. H. Pfeiffer, C. Va´zquez, V. H. Lara, and P. Bosch, Chem. Mater., 2007, 19, 922.
21. D. Bonenfant, M. Mimeault, and R. Hausler, Ind. Eng. Chem. Res., 2007, 46, 8968.
22. T. C. Drage, A. Arenillas, K. M. Smith, C. Pevida, S. Piippo, and C. E. Snape, Fuel, 2007, 86, 22.
23. R. P. S. Chaplin and A. A. Wragg, Journal of Applied Electrochemistry, 2003, 33, 1107.
24. T. Saeki, K. Hashimo, N. Kimura, K. Omata, A. Fujishima, Journal of Electroanalytical Chemistry,1996, 404, 299.
25. N. Spataru, K. Tokuhiro, C. Terashima, T. N. Rao, and A. Fujishima, Journal of Applied Electrochemistry, 2003, 33, 1205.
26. Y. Hori, H. Ito, K. Okano, and K. Nagasu, S. Sato, Electrochimica Acta, 2003, 48, 2651.

27. H. Yano, T. Tanaka, M. Nakayama, and K. Ogura, Journal of Electroanalytical Chemistry, 2004, 565, 287.
28. R. Aydin and F. Köleli, Synthetic Metals, 2004, 144, 75.
29. S. Kaneco, H. Katsumata, T. Suzuki, and K. Ohta, Energy & Fuels, 2006, 20, 409.
30. F. Koleli, T. Atilan, N. Palamut, A.M. Gizir, R. Aydin, and C. H. Hamann, Journal of Applied Electrochemistry, 2003, 33, 447.
31. N. Serpone and E. Pelizzetti, Photocatalysis; Fundamentals and Applications, 1989, 9.
32. H. Yang, J. Ouyang, A. Tang, Y. Xiao, X. Li, X. Dong, and Y. Yu, Materials Research Bulletin, 2006, 1310.
33. L. Andronic and A. Duta, Thin Solid Films, 2007, 515, 6294.
34. J. Liu, F. Gao, X. Chen, K. Yin, S. Dong, Z. Ren, F. Yuan, T. Yu, and Z. Zou, Advanced Materials, 2007, 19, 2889.
35. K. M. Parida, N. Sahu, N. R. Biswal, B. Naik, and A. C. Pradhan, Journal of Colloid and Interface Science, 2008, 318, 231.